Neurobiology of Disease

A Gating Mutation in Ryanodine Receptor Type 2 Rescues Phenotypes of Alzheimer's Disease Mouse Models by Upregulating Neuronal Autophagy

Hua Zhang,[1] Caitlynn Knight,[1] S.R. Wayne Chen,[2] and Ilya Bezprozvanny[1,3]

[1]Department of Physiology, UT Southwestern Medical Center, Dallas, Texas 75390, [2]Department of Physiology and Pharmacology, University of Calgary, Calgary, Alberta T2N 1N4, Canada, and [3]Laboratory of Molecular Neurodegeneration, St. Petersburg State Polytechnical Universty, St. Petersburg 195251, Russian Federation

It is well established that ryanodine receptors (RyanRs) are overactive in Alzheimer's disease (AD), and it has been suggested that inhibition of RyanR is potentially beneficial for AD treatment. In the present study, we explored a potential connection between basal RyanR activity and autophagy in neurons. Autophagy plays an important role in clearing damaged organelles and long-lived protein aggregates, and autophagy dysregulation occurs in both AD patients and AD animal models. Autophagy is known to be regulated by intracellular calcium (Ca^{2+}) signals, and our results indicated that basal RyanR2 activity in hippocampal neurons inhibited autophagy through activation of calcineurin and the resulting inhibition of the AMPK (AMP-activated protein kinase)–ULK1 (unc-51-like autophagy-activating kinase 1) pathway. Thus, we hypothesized that increased basal RyanR2 activity in AD may lead to the inhibition of neuronal autophagy and accumulation of β-amyloid. To test this hypothesis, we took advantage of the RyanR2-E4872Q knock-in mouse model (EQ) in which basal RyanR2 activity is reduced because of shortened channel open time. We discovered that crossing EQ mice with the APPKI and APPPS1 mouse models of AD (both males and females) rescued amyloid accumulation and LTP impairment in these mice. Our results revealed that reduced basal activity of RyanR2-EQ channels disinhibited the autophagic pathway and led to increased amyloid clearance in these models. These data indicated a potential pathogenic outcome of RyanR2 overactivation in AD and also provided additional targets for therapeutic intervention in AD. Basal activity of ryanodine receptors controls neuronal autophagy and contributes to development of the AD phenotype.

Key words: **amyloid; autophagy; calcium; ryanodine receptor; transgenic**

Significance Statement

It is well established that neuronal autophagy is impaired in Alzheimer's disease (AD). Our results suggest that supranormal calcium (Ca^{2+}) release from endoplasmic reticulum contributes to the inhibition of autophagy in AD and that reduction in basal activity of type 2 ryanodine receptors disinhibits the neuronal autophagic pathway and leads to increased amyloid clearance in AD models. Our findings directly link neuronal Ca^{2+} dysregulation with autophagy dysfunction in AD and point to additional targets for therapeutic intervention.

Introduction

Alzheimer's disease (AD) is an age-related brain disorder that causes progressive neurodegeneration predominantly in the cortical and hippocampal brain regions. Major hallmarks of AD are the progressive impairment of memory storage and the accumulation of fibrillary amyloid plaques in patient's brains. Despite decades of research and effort, there is still no effective disease-modifying treatment for AD. Although amyloid pathology is a hallmark and defining feature of AD, targeting the amyloid pathway has been very challenging because of low efficacy and serious side effects. Alternative approaches or mechanisms for memory loss in AD need to be considered as potential therapeutic targets. Increasing studies suggest that neuronal calcium (Ca^{2+}) dysregulation plays an

Received Sep. 23, 2022; revised Nov. 26, 2022; accepted Dec. 19, 2022.

Author contributions: H.Z., C.K., and I.B. designed research; H.Z., C.K., and I.B. performed research; S.R.W.C. contributed unpublished reagents/analytic tools; H.Z., C.K., and I.B. analyzed data; H.Z., C.K., and I.B. wrote the paper.

This research was funded by National Institutes of Health Grants R56-AG-071310 (to I.B.) and R01-AG-055577 (to I.B.), Russian Science Foundation Grant 20-45-01004 (to I.B.), and Canadian Institutes of Health Research Grant PJT-152914 (to S.R.W.C.). I.B. holds the Carl J. and Hortense M. Thomsen Chair in Alzheimer's Disease Research. We thank Dr. Meewhi Kim and Dr. Volodya Zhemkov for comments on the manuscript and helpful discussions.

I.B. is a member of the scientific advisory board of Neurodon, LLC. S.R.W.C. filed a Patent Cooperation Treaty application for "Methods of Treating and/or Preventing Alzheimer's Disease with R-carvedilol." The authors declare no other competing financial interests.

Correspondence should be addressed to Ilya Bezprozvanny at Ilya.Bezprozvanny@UTSouthwestern.edu.

https://doi.org/10.1523/JNEUROSCI.1820-22.2022

important role in AD pathology (Bezprozvanny and Mattson, 2008; Popugaeva et al., 2015; Briggs et al., 2017). The expression and function of ryanodine receptor 2 (RyanR2), an intracellular Ca^{2+} release channel abundantly expressed in the hippocampus (HPC) and cortex (Furuichi et al., 1994; Giannini et al., 1995), are increased in animal models of familial AD (FAD) and in patients with early-stage sporadic AD (Kelliher et al., 1999; Smith et al., 2005; Chakroborty et al., 2009; Zhang et al., 2010; Bruno et al., 2012; Oulès et al., 2012; Liu et al., 2014; Lacampagne et al., 2017). Pharmacological inhibitors of RyanR such as dantrolene demonstrated beneficial effects in a variety of AD cellular and animal models (Chakroborty et al., 2012; Oulès et al., 2012; Peng et al., 2012; Lacampagne et al., 2017). In our previous studies, we used a genetic strategy and evaluated the effects of RyanR3 knockout (Liu et al., 2014) and a gating mutation in RyanR2 (Yao et al., 2020; Liu et al., 2021; Sun et al., 2021) in the context of AD mouse models. Some investigators suggested a mechanism that involves the rescue of neuronal hyperexcitability in AD mice (Liu et al., 2014; Yao et al., 2020; Liu et al., 2021; Sun et al., 2021), some suggest that blocking RyanR-mediated Ca^{2+} leakage may lead to decreased endoplasmic reticulum (ER) stress (Nakamura et al., 2021), some focused on the role of RyanR-mediated Ca^{2+} changes in synaptic function (Chakroborty et al., 2012); some suggested dantrolene can decrease β-secretase and γ-secretase activities and APP phosphorylation by affecting Cdk5 and GSk3β kinase activities (Oulès et al., 2012).

In this article, we would like to propose an alternative model that is based on direct connection between ER Ca^{2+} signaling and neuronal autophagy. Autophagy plays an important role in clearing damaged organelles and long-lived protein aggregates, and a substantial amount of evidence indicates that autophagy dysregulation occurs in both AD patients and animal models (Cataldo et al., 2004; Nixon et al., 2005; Yu et al., 2005; Boland et al., 2008; Yang et al., 2011; Sanchez-Varo et al., 2012; Liu and Li, 2019; Kuang et al., 2020; Chen et al., 2021; Zhang et al., 2021; Mustaly-Kalimi and Stutzmann, 2022). Autophagy is regulated by intracellular Ca^{2+} signals arising from different organelles, including ER and lysosomes. The role of inositol 1,4,5-trisphosphate receptors ($InsP_3Rs$) in the regulation of autophagy had been intensively studied in nonexcitable cells, and $InsP_3R$-mediated Ca^{2+} signals have been suggested to be involved in both inhibitory and stimulatory effects on autophagy (Lam et al., 2008; Cárdenas et al., 2010; Khan and Joseph, 2010; Decuypere et al., 2011a; 2011b; Valladares et al., 2018; Sukumaran et al., 2021). However, the role of RyanR in regulating autophagy is much less studied (Vervliet et al., 2017; Vervliet, 2018). Previous studies were mainly performed by overexpressing RyanRs in nonexcitable cells (Vervliet et al., 2017), or by using pharmacological modulators of RyanR activity that may exert off-target effects (Chung et al., 2016; Qiao et al., 2017; Law et al., 2019). As discussed in a recent review (Vervliet, 2018), a major issue in studying the role of RyanR in autophagy has been the lack of easy-to-use cellular models that express endogenous RyanR. As autophagy is easily influenced by many factors, expressing high levels of exogenous RyanR in cells that do not have adequate RyanR regulators may alter autophagy and other processes and introduce a variety of artifacts.

To resolve these problems in the present study we took advantage of RyanR2-E4872Q knock-in (KI) mouse model (EQ) in which RyanR2 activity is reduced because of shortened channel open time (Chen et al., 2014). Use of this model enabled us to evaluate the consequences of the reduction of endogenous RyanR2 activity in neuronal cells on autophagy and on AD-related phenotypes. The hypothesis that upregulated RyanR expression and activity in AD may be linked to autophagy dysregulation has been proposed previously (Vervliet et al., 2017; McDaid et al., 2020), but it has never been directly tested. Our results suggested that basal activity of RyanR2 inhibits autophagy via activation of calcineurin (CaN), which in turn inhibits the AMP-activated protein kinase (AMPK)–unc-51-like autophagy-activating kinase 1 (ULK1) pathway. Our results further suggested that reduced basal activity of RyanR2 in EQ mice reduced steady-state CaN activity, disinhibited autophagic pathway, and led to amyloid clearance and rescue of AD phenotype in APPKI and APPPS1 mouse models of AD. These data provided a novel pathogenesis signaling pathway for RyanR overactivation in a variety of AD models and may also provide additional targets for therapeutic manipulation in AD.

Materials and Methods

Mice. The generation and characterization of RyanR2-E4872Q (EQ) mice was previously described (Chen et al., 2014). APPKI mice were provided by Takaomi Saido (RIKEN, Wako, Japan; Saito et al., 2014) and used in our previous studies (Zhang et al., 2016). APPPS1 mice (APPK670N; M671L; PS1L166P; Radde et al., 2006) were provided by Mathias Jucker (Tübingen University, Tübingen, Germany) and were also used in our previous studies (Zhang et al., 2010) . The colonies of all lines (on C57BL/6 background) were established at the University of Texas Southwestern Medical Center (UTSW) specific pathogen free barrier facility. Wild-type (WT) C57BL/6 were used in experiments as control mice. All procedures involving mice were approved by the Institutional Animal Care and Use Committee of UTSW, in accordance with the National Institutes of Health *Guidelines for the Care and Use of Laboratory Animals*. Both male and female mice were used in this study, and both sexes were balanced between groups, all the data presented are combined results from both sexes.

Materials. FUW mCherry-GFP-LC3 (plasmid catalog #110060; Leeman et al., 2018) was obtained from Addgene. The lentivirus was generated by cotransfection of shuttle vectors with human immunodeficiency virus-1 packaging vector 8.9 and vesicular stomatitis virus glycoprotein G envelope glycoprotein plasmids into the packaging cell line HEK293T, as we described previously (Zhang et al., 2010).

Western blotting. All protein samples were boiled at 95°C for 5 min, proteins were separated by SDS-PAGE and analyzed by Western blotting with the following antibodies: anti-LC3 (1:1000; catalog #NB100-2220, Novus Biologicals); anti-GAPDH (1:1000; catalog #MAB374, Millipore); anti-APP (1:2000; catalog #A8717, Sigma-Aldrich); anti-phospho-ULK1 (Ser555; D1H4) rabbit mAb (1:1000; catalog #5869, Cell Signaling Technology); anti-ULK1 (D8H5) rabbit mAb (1:1000; catalog #8054, Cell Signaling Technology); anti-phospho-AMPKα (Thr172; 40H9) rabbit mAb (1:1000; catalog #2535, Cell Signaling Technology); anti-AMPKα (D5A2) rabbit mAb (1;1000; catalog #5831, Cell Signaling Technology); anti-tubulin [1:1000; catalog #E7-c, Developmental Studies Hybridoma Bank (DSHB)]; anti-Akt antibody (1:1000; catalog #9272, Cell Signaling Technology); and anti-phospho-Akt (Ser473; 587F11) mouse mAb (1:1000; catalog #4051, Cell Signaling Technology). The HRP-conjugated anti-rabbit (1:3000; catalog #111-035-144) and anti-mouse (1:3000; catalog #115-035-146) secondary antibodies were from Jackson ImmunoResearch. For Western blot analysis, data were densitometrically analyzed using ImageJ software.

Primary hippocampal cultures. The hippocampal cultures were established from postnatal day 0–1 pups and maintained in culture as we described previously (Zhang et al., 2010). Lenti-mCherry-GFP-LC3 infected neurons at 7 d *in vitro* (DIV7); at DIV15–16 cultures were treated with bafilomycin (BAF), ryanodine, FK506, or compound C for

4 h, then were lysed with 1× SDS-PAGE loading buffer for Western blot or fixing of the cells for confocal imaging.

Fura-2 calcium imaging. DIV15–16 hippocampal cultures were maintained in artificial CSF (aCSF) as follows (in mM): 140 NaCl, 5 KCl, 1 MgCl2, 2 CaCl2, and 10 HEPES, at pH 7.3. The cells were loaded with fura-2 AM dye, and 340:380 nm ratio images were collected using a DeltaRAM-X illuminator, an IC-300 camera, and IMAGEMASTER PRO software (all from Photon Technology International). The region of interest used in the image analysis corresponded to the entire cell soma.

β-amyloid 40 and β-amyloid 42 measurements in hippocampal neuronal culture medium. The hippocampal culture medium was collected at DIV15, and β-amyloid 40 (Aβ40) and Aβ42 concentrations were measured by ELISA (kit #KHB3481 and kit #KHB3441, Thermo Fisher Scientific) by following the instructions of the manufacturer. Since the corresponding cultures extract protein and use GAPDH Western blot as a loading control, Aβ40 and Aβ42 concentrations were normalized to their corresponding loading control for comparison between different culture wells.

Aβ40 and Aβ42 measurements from brain cortex homogenization. Brain homogenization followed the instructions in the Thermo Fisher Scientific ELISA kits #KHB3481 and #KHB3441, which used 5 M guanidine HCl and 50 mM Tris HCl, at pH 8.0; the protein concentration was measured; the extract solutions were series diluted; Aβ40 and Aβ42 concentrations were measured using Thermo Fisher Scientific ELISA kits #KHB3481 and #KHB3441); and the data presented as Aβ40 and Aβ42 concentrations were normalized to their corresponding protein concentrations.

Immunohistochemistry. Mice were terminally anesthetized and perfused transcardially with cold PBS followed by fixative (4% paraformaldehyde in PBS, pH 7.4). All brains were removed from skull and weighed. The brains were postfixed overnight at 4°C in 4% paraformaldehyde and equilibrated in 20–30% (w/v) sucrose in PBS. The brains were sliced into 50-μm-thick horizonal sections using a sliding microtome (model SM2000R, Leica). The brain sections were spaced 400 μm apart throughout from the position around interaural 4.96 to interaural 3.76, stained with rabbit anti-LC3 (1:250; catalog #12741, Cell Signaling Technology), rat anti-LAMP1 (1:250; catalog #1D4B, DSHB), and mouse anti-map2 (1:1000; catalog #mAB378, Chemicon), and followed by Alexa Fluor-488 secondary anti-rabbit IgG, Alexa Fluor-561 secondary anti-rat IgG, and Alexa Fluor-633 secondary anti-mouse IgG. Images visualized using a fluorescent confocal microscope (Leica) with a 63× oil-immersion objective. Acquisition parameters (such as laser power and gain) were kept constant for different samples. Image analysis was performed by using the ImageJ analysis software (Molecular Devices), threshold was kept constant for different samples. LC3 and LAMP1 puncta density were only analyzed in hippocampal CA1 neuron cell body layer region. Colocalization of LC3 with LAMP1 analysis was performed using the Coloc2 plugin.

Amyloid plaque staining. The 50 μm horizontal brain sections spaced 400 μm apart throughout from the position around interaural 4.96 to interaural 3.76 were stained with 6E10 anti-Aβ mAb (1:1000; catalog #SIG-39300, Covance), followed Alexa Fluor-488 secondary anti-mouse IgG (1:2000). The quantitative analysis of amyloid load was performed blindly using the IsoCyte laser scanning system (Molecular Devices). The average intensity of the fluorescent signal of the plaques and the number of plaques in cortical and hippocampal areas were calculated automatically for each slice by using ImageJ analysis software (Molecular Devices).

Brain slice field recording. Brain slices were prepared from 6-month-old animals of either sex. Mice were anesthetized and transcardially perfused with dissection buffer before decapitation. The brain was removed, dissected, and sliced in ice-cold dissection buffer containing the following (in mM): 2.6 KCl, 1.25 NaH_2PO_4, 26 NaHCO3, 0.5 CaCl2, 5 MgCl2, 212 sucrose, and 10 dextrose, using a vibratome (model VT 1000S, Leica). The 400 μm horizontal slices, which included HPC and lateral entorhinal cortex (LEC), were collected and transferred into a reservoir chamber filled with aCSF containing the following (in mm): 124 NaCl, 5 KCl, 1.25 NaH_2PO_4, 26 NaHCO3, 2 CaCl2, 1 MgCl2, and 10 dextrose. Slices were allowed to recover for 2–5 h at 30°C. aCSF and dissection buffer were equilibrated with 95% O_2/5% CO_2. For recording, slices were transferred to a submerged recording chamber, maintained at 30°C, and perfused continuously with aCSF at a rate of 2–3 ml/min. Field potentials were recorded with extracellular recording electrodes (1 MΩ) filled with aCSF. The stimulation and recording pipettes were positioned in the outer molecular layer along the lateral perforant pathway (LPP). The function of LPP was validated by measurements of paired-pulse facilitation using 50 ms intervals between pulses as described previously (Colino and Malenka, 1993). Stimulus current was adjusted so that fEPSP stabilized at 40–50% of maximum. Baseline was recorded for at least 20 min until the differences among fEPSP slopes were within 10%. LEC–DG long-term potentiation (LTP) was induced by two bursts of high frequency stimulation (HFS) at 100 Hz for 1 s with 1 min intervals between pulses. Synaptic responses were recorded for at least 60 min after tetanization and quantified as the slope of the evoked fEPSP normalized to the baseline.

Statistical analysis. Statistical comparisons of results obtained in experiments were performed by unpaired *t* test or one-way ANOVA with a Tukey's HSD *post hoc* test. The *p* values are indicated in the text and figure legends, as appropriate. The differences between control and experimental groups were determined to be nonsignificant in cases in which $p > 0.05$.

Data availability. All data are available in the main text.

Results

RyanR2-E4872Q (EQ) mutation increases autophagic flux in primary hippocampal neuronal cultures

To quantify autophagy in primary hippocampal neuronal cultures, we performed Western blotting experiments with antibodies against autophagic marker LC3II (Klionsky et al., 2021). The experiments were performed with lysates prepared from neurons maintained in normal culture media or treated with 400 nM lysosomal acidification inhibitor bafilomycin A1 (BAF) for 4 h. Robust autophagic flux in neurons has been previously reported on the basis of high LC3I/II ratio and accumulation of LC3II with BAF treatment (Rubinsztein et al., 2009; Klionsky et al., 2021). Once LC3-II is formed in neuronal cultures, it is quickly degraded by autophagic flux, and, in contrast with most other cell types, comparison of basal levels of LC3-I and LC3-II is not appropriate because of very low steady-state levels of LC3-II. Thus, in our studies we normalized LC3II (BAF) signal to GADPH loading control to reveal how much LC3-II is actually induced, and to quantify autophagic flux we calculated a ratio of LC3II(BAF)-LC3II(CON)/LC3II(BAF) for each culture treatment (Rubinsztein et al., 2009; Klionsky et al., 2021). In our experiments, we did not observe a significant change in LC3II(BAF)/GAPDH levels, although there is a trend that in APPKI neurons this ratio is slightly higher than in WT, and in EQ neurons this ratio is also slightly higher than in the corresponding control groups (Fig. 1*A*,*B*). However, we observed a significant increase in autophagic flux in EQ neurons when compared with wild-type neurons (Fig. 1*A*,*B*). When similar analysis was performed with primary neuronal cultures from APPKI mice and APPKI;EQ mice, we discovered that autophagic flux is somewhat reduced in APPKI neurons (this change did not reach a level of statistical significance), but autophagic flux is significantly enhanced in APPKI;EQ neurons (Fig. 1*A*,*B*).

To further evaluate autophagy in these neuronal cultures, we infected hippocampal neurons with lentiviruses encoding the mCherry-GFP-LC3 reporter construct (Leeman et al., 2018). The GFP signal is sensitive to the acidic and/or proteolytic conditions of the lysosome lumen, whereas mCherry is more stable. As a

result, colocalization of GFP and mCherry fluorescence (visible as yellow) indicates a compartment that has not yet fused with a lysosome, such as autophagosome (AP; Leeman et al., 2018). In contrast, mCherry signal without GFP (free red) corresponds to an acidic autolysosome (AL; Leeman et al., 2018). If the cell autophagy flux is high, the GFP signal would be quenched in the lysosome, resulting in the low Yellow/Red ratio (Y/R%). In contrast, if the autophagy flux is low, then we expect to see more yellow puncta. Thus, the Y/R% observed with this indicator is inversely proportional to the autophagic flux in a cell. The results of our experiments confirmed that hippocampal neurons have constitutively robust autophagic flux (most puncta are free red puncta, with very low Y/R ratio; Fig. 1*C*, *D*). Comparison of Y/R ratios among WT, EQ, APPKI, and APPKI:EQ neurons suggested that there is a trend that EQ have higher flux than WT, and APPKI flux is slightly more impaired than WT, but these changes did not reach the level of significance (Fig. 1*D*). However. we found autophagic flux in APPKI;EQ neurons was significantly increased when compared with APPKI neurons (Fig. 1*D*). These conclusions are in agreement with the results of LC3II Western blotting analysis (Fig. 1*A*,*B*).

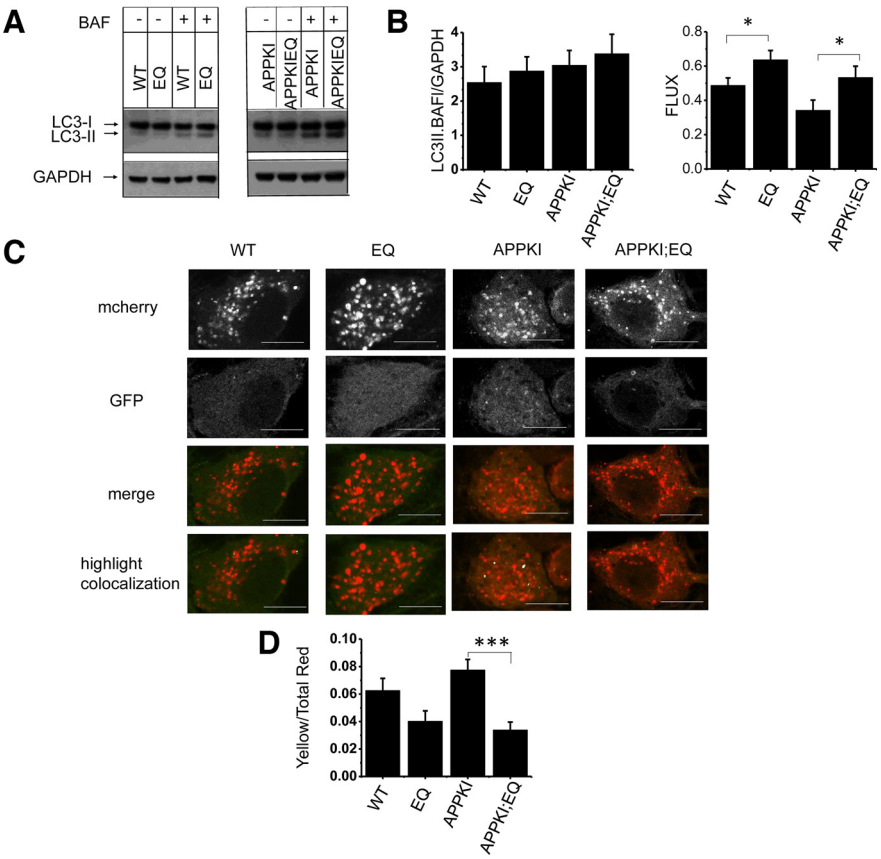

Figure 1. RyanR2-E4872Q (EQ) mutation increases autophagic flux in primary hippocampal neuronal cultures. ***A***, Western blot staining of lysates prepared from wild-type, EQ, APPKI, and APPKI;EQ primary hippocampal neuronal culture at DIV15 with (+) or without (–) 4 h treatment with BAF. The blots were stained with antibodies against autophagic marker LC3 and with GAPDH as loading control. LC3-I and LC3-3-II forms were detected as indicated. ***B***, An average intensity of LC3-II staining in the presence of BAF (normalized to GAPDH intensity for each sample) is shown for wild-type, EQ, APPKI, and APPKI;EQ lysates. An average autophagic flux calculated as LC3II(BAF)-LC3II(CON)/LC3II(BAF) for each sample is shown for wild-type, EQ, APPKI, and APPKI;EQ lysates. The data are shown as the mean ± SE ($n \geq 11$ cultures). *$p < 0.05$, one-way ANOVA with Tukey's *post hoc* test. ***C***, Representative confocal images of wild-type, EQ, APPKI, and APPKI;EQ primary hippocampal neuronal cultures infected with Lenti-mCherry-GFP-LC3 viruses. The images are shown for red (mCherry) and green (GFP) channels, a merged red/green channel (merge), and a highlighted colocalization image with white color using the FUJI colocalization plugin. Scale bar, 5 μm. ***D***, An average Y/R ratio is shown for wild-type ($N = 61$), EQ ($N = 46$), APPKI ($N = 112$), and APPKI;EQ ($N = 84$) neurons from three batches of cultures. The data are shown as the mean ± SE. ***$p < 0.001$, one-way ANOVA with Tukey's *post hoc* test.

Basal RyanR2 activity regulates autophagy by modulating CaN-pAMPK–pULK1 pathway

The E4872Q (EQ) mutation in RyanR2 shortens channel open times (Chen et al., 2014), and we predicted that it should lead to a reduction of basal Ca^{2+} flux from the ER and reduced levels of neuronal cytosolic Ca^{2+} in the steady state. To test this hypothesis, we performed fura-2 imaging experiments and quantified basal cytosolic Ca^{2+} levels in wild-type, EQ, APPKI, and APPKI;EQ hippocampal neuronal cultures. We discovered that APPKI neurons have significantly higher basal Ca^{2+} levels than wild-type neurons, and EQ mutation significantly decreased basal Ca^{2+} levels in both EQ and APPKI;EQ neurons (Fig. 2*A*). Thus, we reasoned that enhanced autophagic flux in EQ and APPKI;EQ neurons (Fig. 1) may be because of reduced basal ER Ca^{2+} flux from the ER and reduced basal cytosolic Ca^{2+} levels. To test this hypothesis, we inhibited RyanR activity by treating wild-type, EQ, APPKI, and APPKI;EQ neurons with 50 μM ryanodine for 4 h in the presence and absence of BAF. The autophagy and autophagic flux were quantified by Western blotting of neuronal lysates for LC3II, as described above. Obtained results indicated that pharmacological inhibition of RyanR significantly increased autophagic flux in wild-type and APPKI neurons, but not in EQ and APPKI;EQ neurons (Fig. 2*B*,*C*), supporting our hypothesis regarding a role of RyanR in the control of neuronal autophagy. It has been reported that increased cytosolic Ca^{2+} is able to activate CaN, which in turn can suppress the AMPK-dependent autophagy pathway in cardiomyocytes (He et al., 2014). To test the importance of CaN in the regulation of neuronal autophagy, we exposed neuronal cultures to specific CaN inhibitor FK506 (1 μM for 4 h) and evaluated autophagy and autophagic flux by LC3II Western blotting of neuronal lysates. In these experiments, we discovered that FK506 was able to stimulate autophagic flux in wild-type and APPKI neurons, but not in EQ and APPKI;EQ neurons (Fig. 2*B*,*C*). Thus, the effects of FK506 were similar to the effects of ryanodine, and both effects were occluded by EQ mutation. To further confirm these findings, we infected neuronal cultures with lentiviruses encoding mCherry-GFP-LC3 reporter construct (Leeman et al., 2018) and performed quantification of autophagic flux by calculating Yellow/Red signal ratio, as described above. In these experiments, we discovered that pharmacological inhibition of RyanR by ryanodine significantly enhanced autophagic flux in APPKI neurons and that the inhibition of CaN by FK506 dramatically enhanced autophagic flux in all groups of neurons (Fig. 2*D*), suggesting a critical role of CaN in the control of neuronal autophagy.

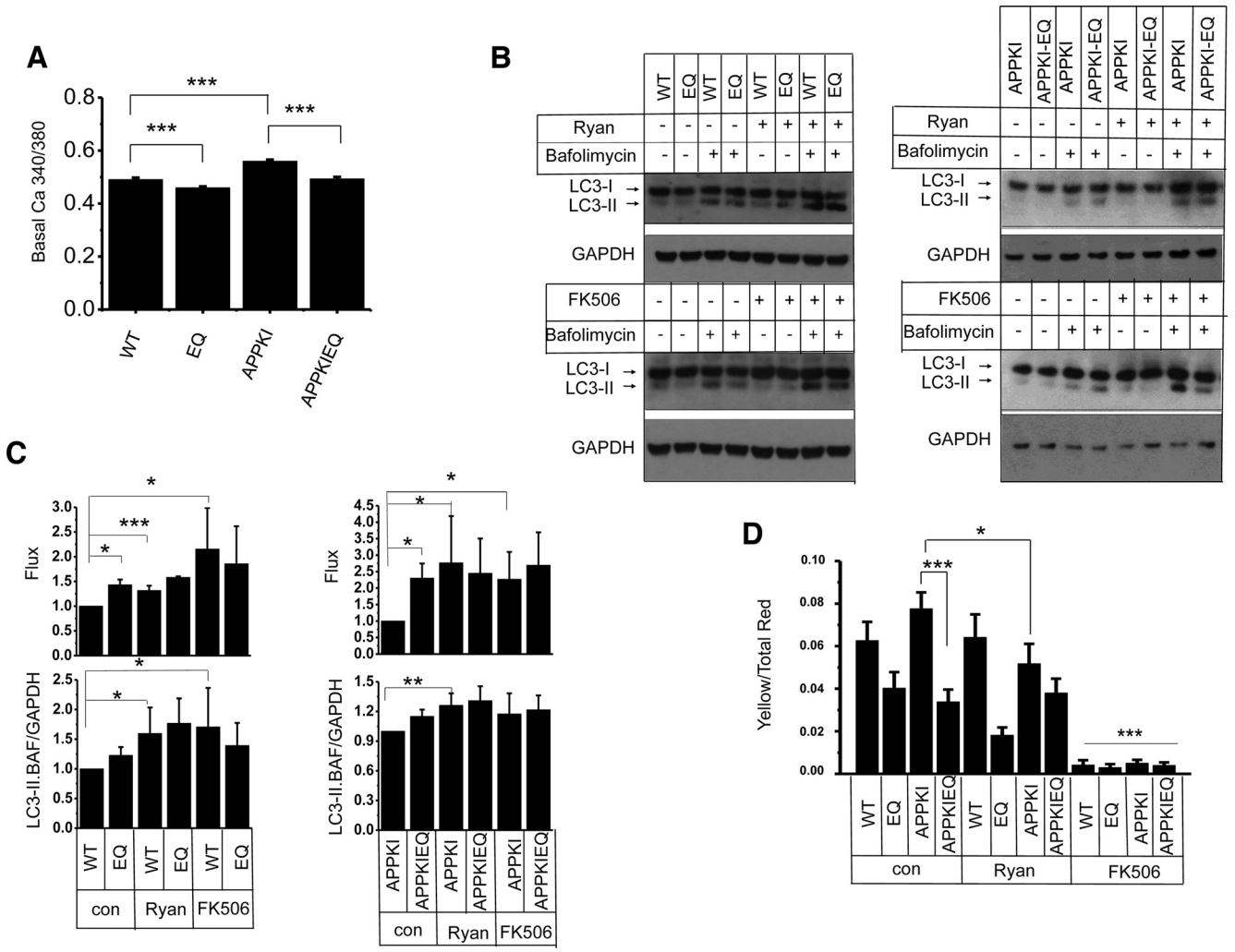

Figure 2. Basal RyanR activity regulates autophagy flux by activating CaN. ***A***, Basal calcium levels in hippocampal neuron cultures. Average basal Ca^{2+} levels reported by 340/380 fura-2 signal ratios in DIV15–16 wild-type, EQ, APPKI, and APPKI;EQ hippocampal neuronal cultures. The data are shown as the mean ± SE ($n \geq 373$ neurons from at least three batches of cultures). ***$p < 0.001$, one-way ANOVA with Tukey's *post hoc* test. ***B***, Western blot staining of lysates prepared from wild-type, EQ, APPKI, and APPKI;EQ primary hippocampal neuronal culture at DIV15 with (+) or without (–) 4 h treatment with BAF, Ryan, or FK506 as indicated. The blots were stained with antibodies against autophagic marker LC3 and with GAPDH as a loading control. LC3-I and LC3-II forms were detected as indicated. ***C***, An average intensity of LC3-II staining in the presence of BAF (normalized to GAPDH intensity for each sample), and an average autophagic flux calculated as LC3II(BAF)-LC3II(CON)/LC3II(BAF) is shown for wild-type, EQ, APPKI, and APPKI;EQ samples with (+) or without (–) 4 h treatment with Ryan or FK506. The data are shown as the mean ± SE ($n \geq 3$ cultures). *$p < 0.05$, **$p < 0.01$, one-way ANOVA with Tukey's *post hoc* test. ***D***, An average Yellow/Red ratio of image density observed in wild-type, EQ, APPKI, and APPKI;EQ cultures infected with Lenti-mCherry-GFP-LC3 viruses in control conditions (con) or after 4 h of treatment with Ryan or FK506. The data are shown as the mean ± SE ($n \geq 25$ neurons from three batches of cultures). *$p < 0.05$, ***$p < 0.001$, one-way ANOVA with Tukey's *post hoc* test.

Activation of CaN has been shown to control autophagy by suppressing activity of AMPK in cardiomyocytes (He et al., 2014). To determine whether a similar signaling pathway operates in neurons, we performed Western blotting experiments with antibodies specific for total AMPK and for the phosphorylated form pAMPK. These experiments were performed with lysates prepared from wild-type, EQ, APPKI, and APPKI;EQ neuronal cultures. In addition to the AMPK pathway, we also evaluated the AKT pathway, which is also known to modulate autophagy through a mammalian target of rapamycin (mTOR)-dependent signaling network (Al-Bari and Xu, 2020). We discovered that the pAKT/AKT ratio was decreased in APPKI neurons, but the EQ mutation did not induce significant changes in pAKT/AKT ratio (Fig. 3*A*,*B*), suggesting that this pathway is not responsible for the increase in autophagic flux observed in EQ neurons. In contrast, the pAMPK/AMPK ratio was significantly increased in EQ neurons (Fig. 3*A*,*B*), and its increase almost reached a level of statistical significance in APPKI;EQ neurons (Figs. 3*A*,*B*). These results supported the hypothesis that basal Ca^{2+} release from ER via RyanR2 modulates levels of neuronal autophagy via CaN–AMPK pathway, which is similar to conclusions reached in studies of autophagy in cardiomyocytes (He et al., 2014). Consistent with this conclusion, we demonstrated that AMPK inhibitor dorsomorphin (compound C; Lu et al., 2014) almost completely blocked the autophagosome fusion with lysosome in neuronal cultures using the mCherry-GFP-LC3 assay (Fig. 3*E*).

In nonexcitable cells, AMPK controls autophagy by phosphorylating and activating ULK1 at position Ser555 (Egan et al., 2011). To determine whether the same pathway is involved in the control of neuronal autophagy, we performed Western blotting experiments with antibodies specific for pULK1-Ser555. We determined that EQ mutation significantly increased the pULK1-Ser555/ULK1 ratio in both wild-type and APPKI neurons (Fig. 3*A*,*B*). To confirm that the activation of AMPK and ULK1 kinases in EQ neurons is indeed because of reduced

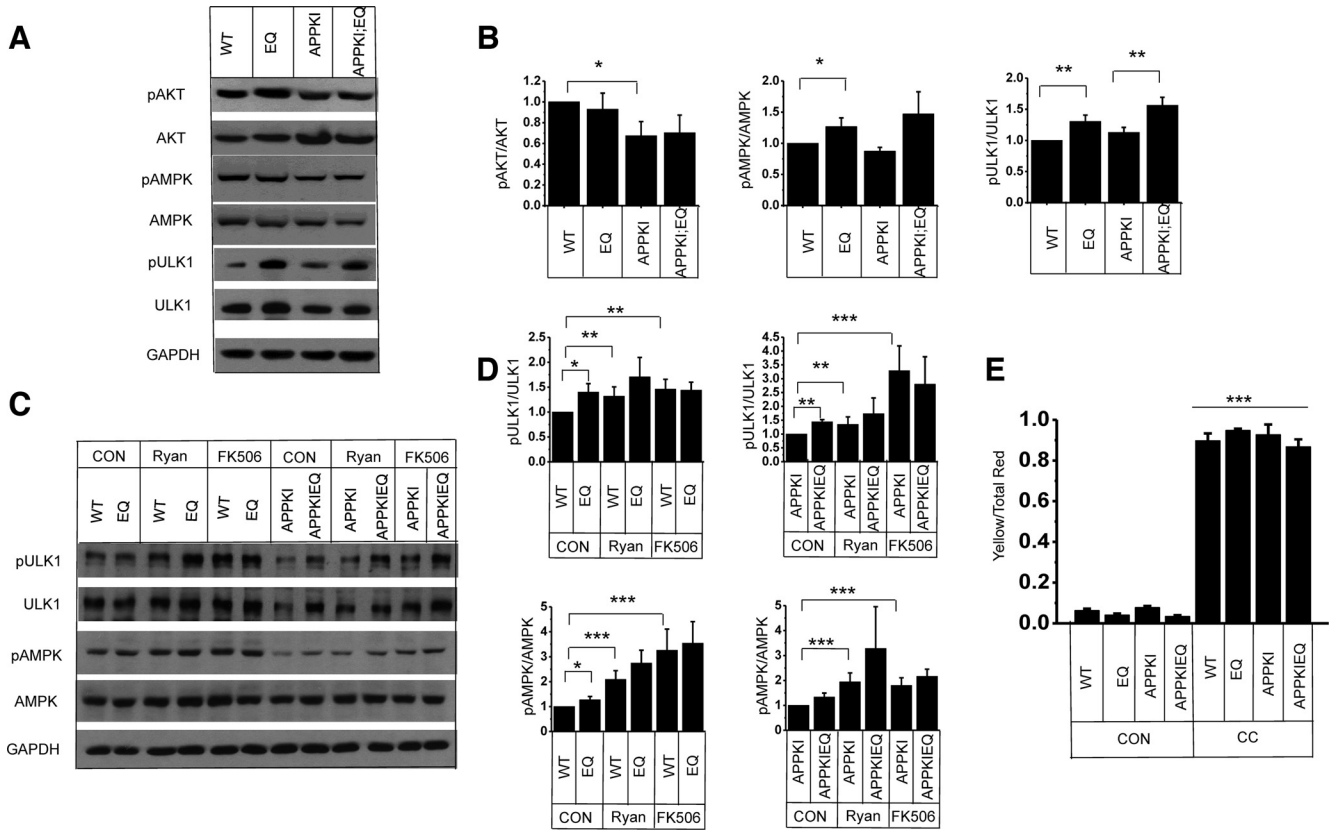

Figure 3. Basal RyanR2 activity regulates autophagy flux by modulating the CaN–pAMPK–pULK1 pathway. ***A***, Western blot staining of lysates prepared from wild-type, EQ, APPKI, and APPKI;EQ primary hippocampal neuronal cultures at DIV15. The blots were stained with antibodies against pAKT and AKT, pAMPK, and AMPK, pULK1 (Ser555), and ULK1, and with GAPDH as a loading control. ***B***, An average ratio of pAKT/AKT, pAMPK/AMPK, and pULK1(Ser555)/ULK1 is shown for wild-type, EQ, APPKI, and APPKI;EQ samples. The data are shown as the mean ± SE ($n \geq 5$ cultures). *$p < 0.05$, **$p < 0.01$, one-way ANOVA with Tukey's *post hoc* test. ***C***, Western blot staining of lysates prepared from wild-type, EQ, APPKI, and APPKI;EQ primary hippocampal neuronal cultures at DIV15 in control conditions (CON) or after 4 h treatment with Ryan or FK506 as indicated. The blots were stained with antibodies against pAMPK and AMPK, pULK1 (Ser555), and ULK1, and with GAPDH as a loading control. ***D***, An average ratio of pAKT/AKT and pULK1(Ser555)/ULK1 is shown for wild-type, EQ, APPKI, and APPKI;EQ samples in control conditions (CON) or after 4 h of treatment with Ryan or FK506 as indicated. The data are shown as the mean ± SE ($n \geq 3$ cultures). *$p < 0.05$, **$p < 0.01$, ***$p < 0.001$, one-way ANOVA with Tukey's *post hoc* test. ***E***, Pharmacological inhibition of AMPK blocks autophagic flux. Average Yellow/Red ratios in wild-type, EQ, APPKI, and APPKI;EQ primary hippocampal cultures infected with Lenti-mCherry-GFP-LC3 viruses in control conditions (con) or after 4 h of treatment with compound C (comp C). The data are shown as the mean ± SE ($n \geq 17$ neurons from four coverslips of cultures); all of the four CC groups are significantly more increased than the four control groups. ***$p < 0.001$, one-way ANOVA with Tukey's *post hoc* test. Note: data from control groups are from the same data as in Figure 1.

RyanR2 and CaN activity, we treated these neurons with ryanodine (50 μM ryanodine for 4 h) or with FK506 (1 μM for 4 h). In these experiments, we observed that ryanodine treatment resulted in increased pAMPK/AMPK and pULK1-Ser555/ULK1 ratios in both wild-type and APPKI neurons (Fig. 3*C*, *D*). However, there was no difference in pAMPK/AMPK or pULK1-Ser555/ULK1 ratios between wild-type and EQ or APPKI and APPKI:EQ in the presence of ryanodine (Fig. 3*C*,*D*). On both readouts, the effects of FK506 treatment were similar to the effects of ryanodine (Fig. 3*C*,*D*). Based on results obtained in this series of biochemical experiments (Figs. 2, 3), we proposed that basal activity of RyanR2 regulates neuronal autophagic flux by activating CaN, which in turn inhibits the pAMPK–pULK1-Ser555 pathway, and that the EQ mutation in RyanR2 can disinhibit this pathway and promote neuronal autophagic flux (Fig. 1).

In addition to regulating the phosphorylation of AMPK, CaN may also enhance the transcription of genes that are involved in autophagy and lysosomal function, such as LC3 and several others (Sardiello et al., 2009; Settembre et al., 2012; Medina et al., 2015) through dephosphorylation of transcription factor EB (TFEB). However, in our experiments EQ mutation did not have a significant effect on the total levels of LC3 (Figs. 1-3) or pTFEB (data not shown), indicating that transcriptional changes are not likely to be responsible for the observed stimulation of autophagy in cultured hippocampal neurons. We also detected the total levels of Beclin 1, a protein involved in the early events of AP formation. We found that neither EQ mutation nor ryanodine or FK506 treatment induced significant changes in Beclin 1 levels (data not shown), consistent with the published data (Vervliet et al., 2017; Vervliet, 2018). However, we cannot fully exclude that RyanR2 activity may also affect earlier steps in the autophagy process via influencing other targets beyond the scope of current study.

RyanR2-E4872Q (EQ) mutation upregulate autophagy pathway *in vivo*

Results obtained in experiments with primary hippocampal neuronal cultures (Figs. 1-3) enabled us to propose the hypothesis that reduced basal Ca^{2+} release from ER because of E4872Q (EQ) gating mutation in RyanR2 leads to the stimulation of neuronal autophagy. To study the autophagy–lysosomal pathway changes *in vivo*, we performed a series of immunostaining experiments with hippocampal slices from 6-month-old mice using antibodies against LC3 and lysosomal marker LAMP1 (Fig. 4*A*). MAP2 staining was used to identify neuronal cells in

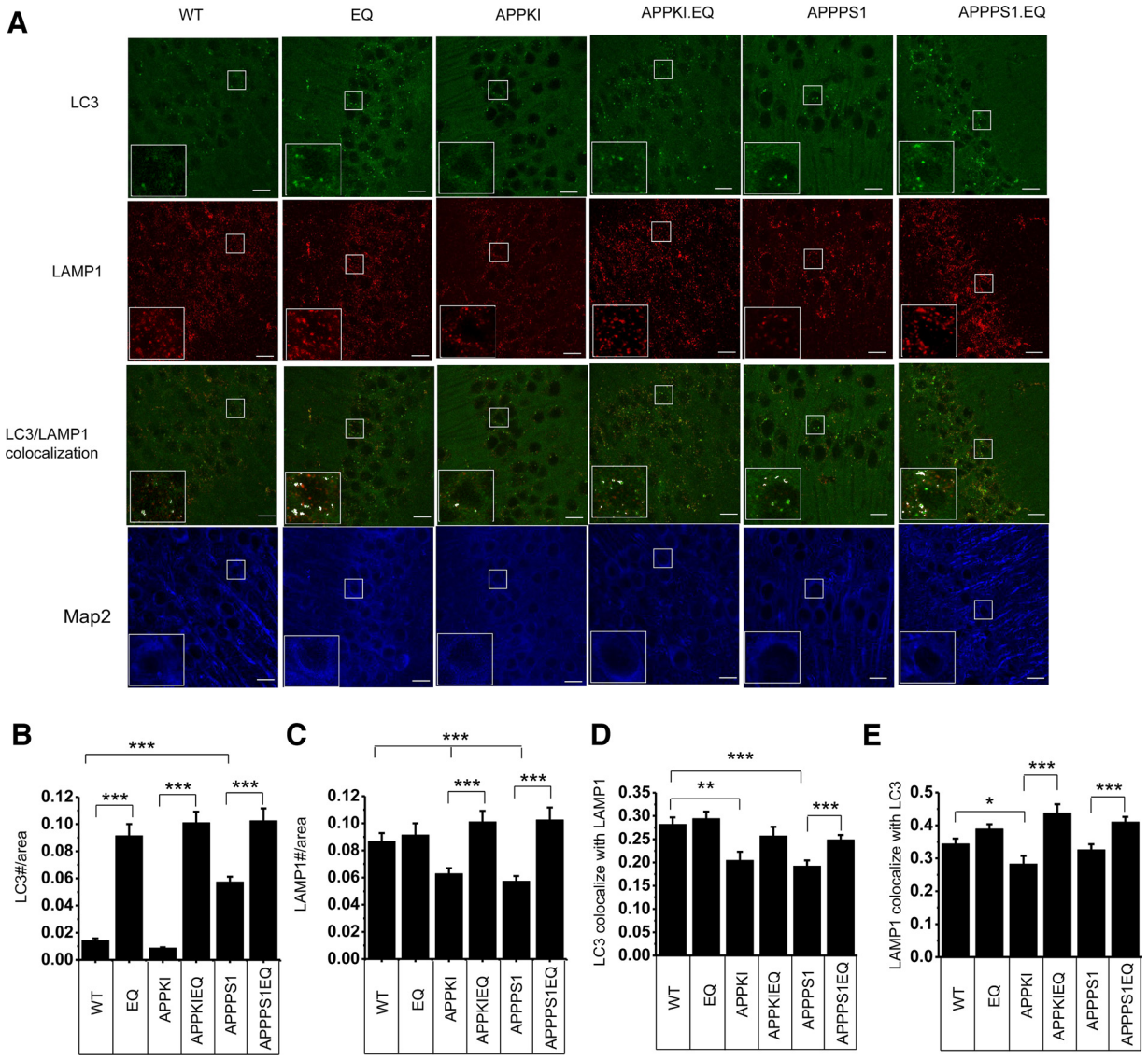

Figure 4. RyanR2-E4872Q (EQ) mutations upregulate the autophagy pathway *in vivo*. ***A***, Representative confocal images of hippocampal CA1 regions from 6-month-old wild-type, EQ, APPKI, APPKI;EQ, APPPS1, and APPPS1;EQ mice stained with antibodies against autophagic marker LC3 (green), lysosomal marker LAMP1 (red) and neuronal marker MAP2 (blue). Higher magnificent images of white box area were shown in the bottom left corner; LC3 and LAMP1 colocalization images were also shown. Colocalization pixels in the box area were highlighted with white color using the FUJI colocalization plugin. Scale bar, 20 μm. ***B***, ***C***, The average of LC3-positive (***B***) and LAMP1-positive (***C***) puncta numbers normalized to CA1 cell body layer area is shown for each strain of mice. The data are shown as the mean ± SE ($n \geq 9$ slices from 5 mice in each group). *$p < 0.05$, **$p < 0.01$, ***$p < 0.001$, one-way ANOVA with Tukey's *post hoc* test. ***D***, MCC of LC3 with LAMP1 puncta in hippocampal CA1 neurons. The data are shown as the mean ± SE ($n \geq 54$ neurons from 5 mice in each group). *$p < 0.05$, **$p < 0.01$, ***$p < 0.001$, one-way ANOVA with Tukey's *post hoc* test. ***E***, MCC of LAMP1 with LC3 puncta in hippocampal CA1 neurons. The data are shown as the mean ± SE ($n \geq 54$ neurons from 5 mice in each group). *$p < 0.05$, **$p < 0.01$, ***$p < 0.001$, one-way ANOVA with Tukey's *post hoc* test.

these experiments (Fig. 4*A*). To quantify these results, we analyzed total LC3 and LAMP1-positive puncta in hippocampal CA1 neurons and calculated a fraction of LC3 colocalized with LAMP1 and the fraction of LAMP1 colocalized with LC3. Similar to experiments with neuronal cultures, we performed experiments with slices from wild-type and EQ mice, as well as from APPKI and APPKI;EQ mice. In addition, we also analyzed APPPS1 and APPPS1;EQ mice. We included APPPS1 mice as it is a more aggressive model of amyloidosis than that in APPKI mice (Radde et al., 2006). APPS1 mice start to accumulate amyloid plaques at a very young age (6–8 weeks), while it takes up to 12 months for amyloid plaques to become visible in brain samples from APPKI mice. Therefore, analysis of these two AD mouse models enabled us to compare signaling pathways acting upstream or downstream of Aβ amyloidosis (Saito et al., 2014). Consistent with results obtained in neuronal cultures, we discovered that EQ mutation resulted in a significant increase in LC3 staining when compared with the wild-type mice (Fig. 4*A*, *B*), suggesting stimulation of neuronal autophagy in these mice. We also discovered that APPPS1 mice have increased LC3 staining when compared with wild-type and APPKI mice (Fig. 4*A*,*B*), consistent with reports that indicated upregulated autophagosome formation as a result of amyloid plaque accumulation (Long et al., 2020). Interestingly, EQ mutation also significantly increased LC3 staining in both APPKI and APPPS1 mouse lines (Fig. 4*B*), suggesting drastic upregulation of autophagy. We also discovered that both APPKI and APPPS1 mice show reduced LAMP1 staining when compared with wild-type mice (Figs. 4*A*,*C*), consistent with the reduced expression of lysosomal markers in the brains of AD

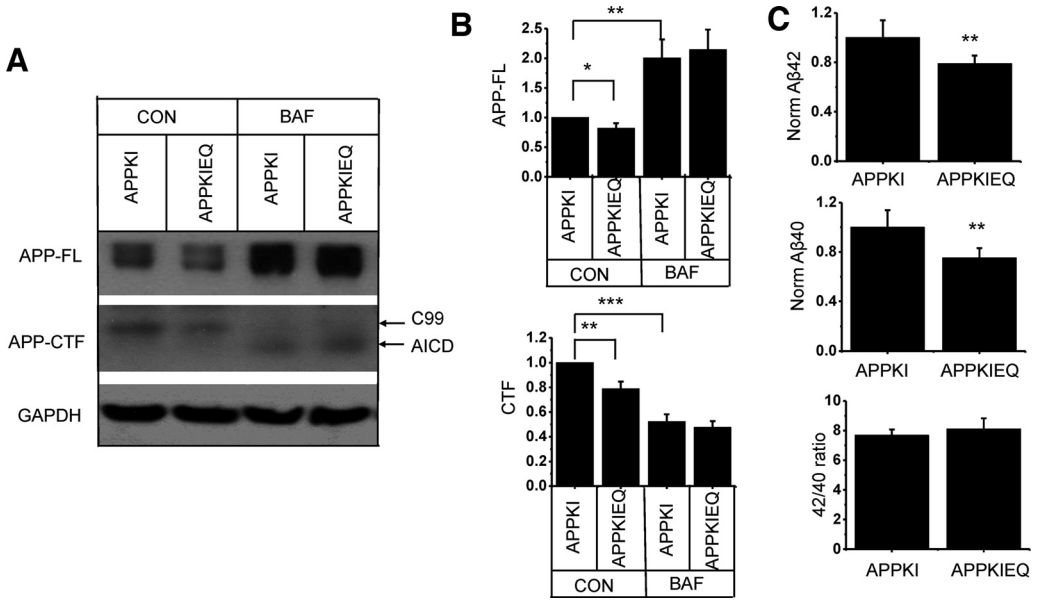

Figure 5. The RyanR2-E4872Q (EQ) mutation promotes APP degradation through the autophagic pathway. ***A***, Western blot staining of lysates prepared from APPKI and APPKI;EQ primary hippocampal neuronal culture at DIV15 with (BAF) or without (CON) 4 h of treatment with bafolimycin 1A. The blots were stained with antibodies against APP and with GAPDH as a loading control. Full-length APP (APP-FL) and APP-CTF were detected, as indicated. ***B***, ***C***, An average intensity of APP-FL (***B***) and APP-CTF (***C***) staining in control conditions (CON) and in the presence of BAF (normalized to GAPDH intensity for each sample) is shown for EQ, APPKI, and APPKI;EQ sample. The data are shown as the mean ± SE ($n \geq 14$ cultures). *$p < 0.05$, **$p < 0.01$, ***$p < 0.001$, one-way ANOVA with Tukey's *post hoc* test. ***D***, Normalized Aβ40, Aβ42 (to cell density loading control), and Aβ42/Aβ40 ratio in the culture media collected from APPKI and APPKI;EQ hippocampal neuronal cultures at DIV15. The data are shown as the mean ± SE ($n = 6$ cultures). **$p < 0.01$, Student's *t* test.

patients and mouse models (Long et al., 2020). Remarkably, EQ mutation rescued the LAMP1 staining signal to the wild-type levels in both AD models (Fig. 4*A*,*C*). We also calculated LC3 colocalization with LAMP1 and LAMP1 colocalization with LC3 using the Manders coefficient of colocalization (MCC) and discovered that MCC values were significantly decreased in both APPKI and APPPS1 hippocampal CA1 neurons, which indicate impaired AL formation (Fig. 4*D*,*E*) . In contrast, EQ mutation significantly rescued this defect in APPS1 mice (Fig. 4*D*,*E*) and showed a rescue trend in APPKI mice ($p = 0.054$; Fig. 4*D*). All of these *in vivo* results suggest that EQ mutations greatly upregulate the autophagy–lysosomal pathway in neurons and that AD neurons display autophagy–lysosomal fusion dysfunction at a very early stage, which can be fully rescued *in vivo* by EQ mutation in RyanR2. This defect and autolysosome acidification defects in AD neurons that have been reported previously (Lee et al., 2010, 2015, 2022; Mustaly-Kalimi and Stutzmann, 2022) may work together in the AD pathogenesis pathway.

RyanR2-E4872Q (EQ) mutation promotes APP and C99 degradation in APPKI neurons

In agreement with the known role of autophagy in the processing of APP (Liu and Li, 2019; Rahman et al., 2021), we discovered that treatment with BAF significantly increased the levels of full-length APP in APPKI neurons (Fig. 5*A*,*B*). Consistent with increased autophagic flux in APPKI;EQ neurons, the levels of full-length APP were significantly decreased in APPKI;EQ neurons (Fig. 5*A*,*B*). APP-C-terminal fragment (CTF; C99) and intracellular C-terminal domain (AICD) fragments of APP proteolysis have been reported to be degraded by the autolysosomal pathway (Vingtdeux et al., 2007). Indeed, we observed the accumulation of AICD following BAF treatment of APPKI and APPKI;EQ neurons (Fig. 5*A*). The levels of the APP-CTF (C99) fragment were reduced in APPKI;EQ neurons (Fig. 5*A*, *C*). However, in bafilomycin-treated neurons, the APP-CTF (C99) fragment levels were greatly decreased (Fig. 5*A*,*C*), most likely because of the inhibition of BACE1-mediated APP processing caused by bafilomycin treatment (Haass et al., 1995; Evrard et al., 2018). We can barely detect C83 fragment from α-cleavage in APPKI neurons because the Swedish mutations in APP facilitate β-cleavage. Consistent with a reduction in APP and APP-CTF (C99) levels, we detected a reduction in Aβ40 and Aβ42 levels in the culture media of APPKI;EQ neurons when compared with APPKI neurons without significant changes in Aβ42/Aβ40 ratio (Fig. 5*D*).

RyanR2-E4872Q (EQ) mutation reduces amyloid plaque accumulation and rescues LTP defects in AD mice

Since we discovered that EQ mutation in RyanR2 promotes APP degradation by autophagy and decreases levels of Aβ40 and Aβ42 in experiments with APPKI neuronal cultures (Fig. 5), we evaluated the effects of EQ mutation on amyloid pathology *in vivo*. In our analysis, we observed a significant reduction in amyloid plaque numbers and intensity in the hippocampal region of 6-month-old APPS1;EQ mice when compared with age-matched APPPS1 mice (Fig. 6*A*,*B*). To understand the reasons for the reduction in plaque load, we prepared homogenates from cortical tissue of 6-month-old APPPS1 and APPPS1;EQ mice and measured the concentration of Aβ42 and Aβ40 by ELISA. We discovered that, in agreement with *in vitro* culture data (Fig. 5), both Aβ42 and Aβ40 levels were significantly decreased in APPPS1;EQ cortical homogenates (Fig. 6*C*). However, we found that the Aβ42/Aβ40 ratio is significantly increased in APPPS1;EQ cortical samples, which we did not observe *in vitro* (Fig. 5*C*). It is possible that changes in the ratio are because of changes in lysosomal function in the aging APPPS1;EQ mice, as it has been shown that cathepsin D changes can regulate this Aβ42/Aβ40 ratio (Suire et al., 2020) or some unknown γ-secretase changes in old APPPS1;EQ mice, which

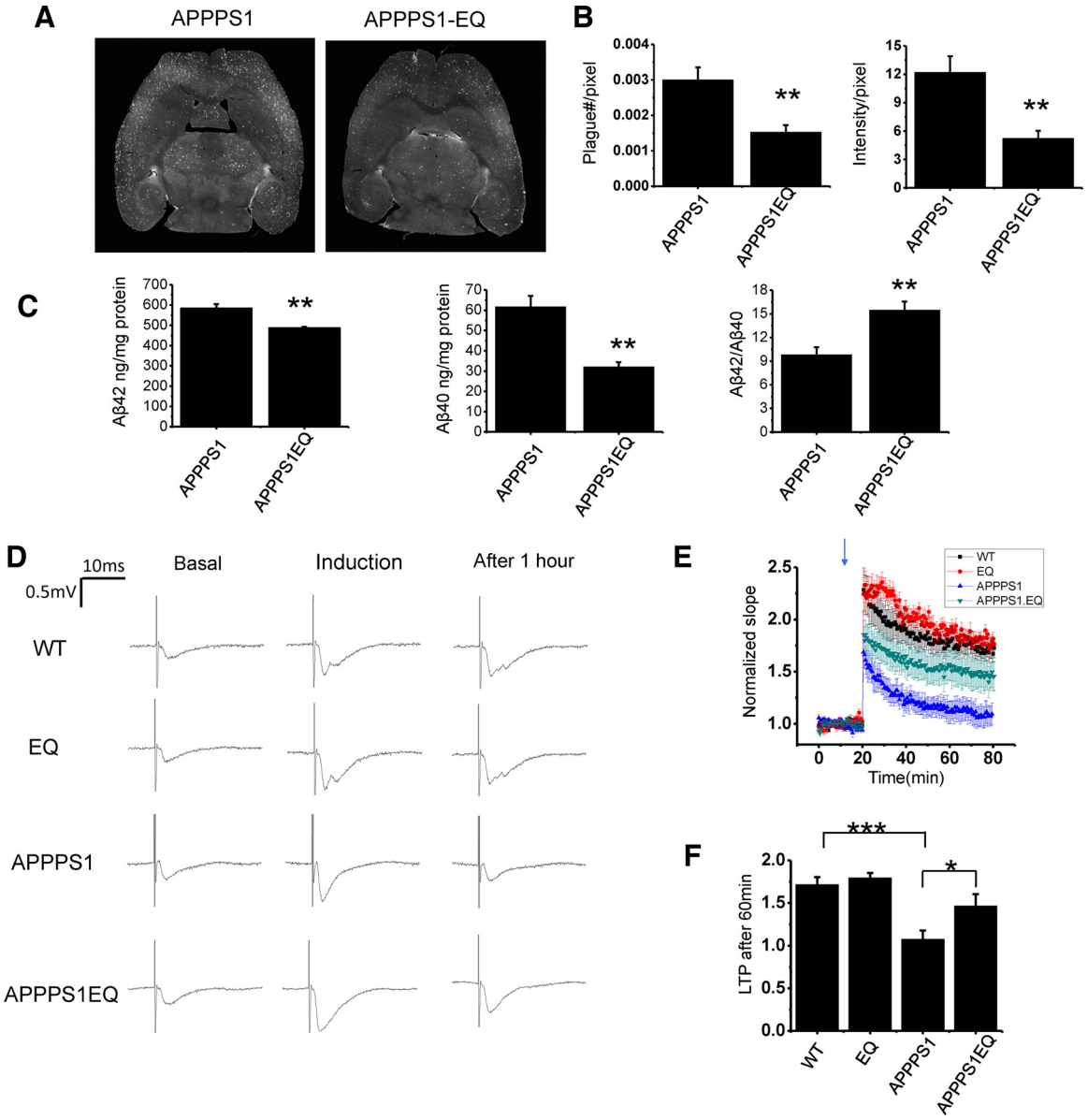

Figure 6. RyanR2-E4872Q (EQ) mutation reduces amyloid plaque accumulation and rescues the LTP defect in APPPS1 mice. ***A***, Representative IsoCyte laser-scanning images of horizontal brain slices from 6-month-old APPPS1 and APPPS1;EQ mice stained with fluorescently labeled 6E10 anti-amyloid antibodies. ***B***, Average density of amyloid plaques and average signal intensity within the plaques for APPPS1 and APPPS1;EQ mice samples. The data are shown as the mean ± SE ($n \geq 10$ mice). $^{**}p < 0.01$, Student's *t* test. ***C***, Normalized Aβ40 concentration, Aβ42 concentration, and Aβ42/Aβ40 ratio in the cortex homogenates collected from 6-month-old APPPS1 and APPPS1;EQ mice. The data are shown as the mean ± SE ($n \geq 5$ mice). $^{**}p < 0.01$, Student's *t* test. ***D***, Sample fEPSP traces are shown for 6-month-old WT, EQ, APPPS1, and APPPS1:EQ brain slices before stimulation (basal), immediately after tetanus stimulation (induction), and 1 h after tetanus stimulation (after 1 h). ***E***, Normalized and averaged slope of fEPSP recorded from 6-month-old hippocampal slices from wild-type, EQ, APPPS1, and APPPS1:EQ mice. The LTP was induced by HFS shown by the arrow. ***F***, Averaged change in normalized fEPSP slope recorded 1 h after HFS for wild-type, EQ, APPPS1, and APPPS1;EQ mice. The data are shown as the mean ± SE ($n \geq 8$ mice). $^{*}p < 0.05$, $^{***}p < 0.001$, one-way ANOVA with Tukey's *post hoc* test.

we can investigated in the future. Because of the less severe phenotype, we compared amyloid load in hippocampal region of 13-month-old APPKI and APPKI;EQ mice. In this analysis, we discovered a trend in the reduction of amyloid plaque numbers and intensity in APPKI;EQ mice that did not reach a level of statistical significance (Fig. 7*A*,*B*), most likely because of the small numbers of plaques observed in this model.

To access the effects of EQ mutation on synaptic function, we performed measurements of LTP using brain slices. The EC–hippocampal circuit is critically involved in memory formation (Buzsáki and Moser, 2013), and dysfunction of this circuit has been identified in the earliest stages of AD. The LEC develops tau tangles and amyloid plaques before other regions of the brain (Braak and Braak, 1991; Braak and Del Tredici, 2015). Consistent with previous reports (Radde et al., 2006; Zhang et al., 2016), we determined that LTP in the lateral perforant pathway was impaired at 6 months of age for both APPPS1 (Fig. 6*C*,*D*) and for APPKI (Fig. 7*C*,*D*) mice when compared with wild-type age-matched mice. Importantly, these LTP defects were rescued in both APPPS1;EQ (Fig. 6*C*,*D*) and APPKI;EQ (Fig. 7*C*,*D*) mice.

Discussion

AD is characterized by the accumulation of abnormal protein aggregates including amyloid plaques (composed of Aβ peptides)

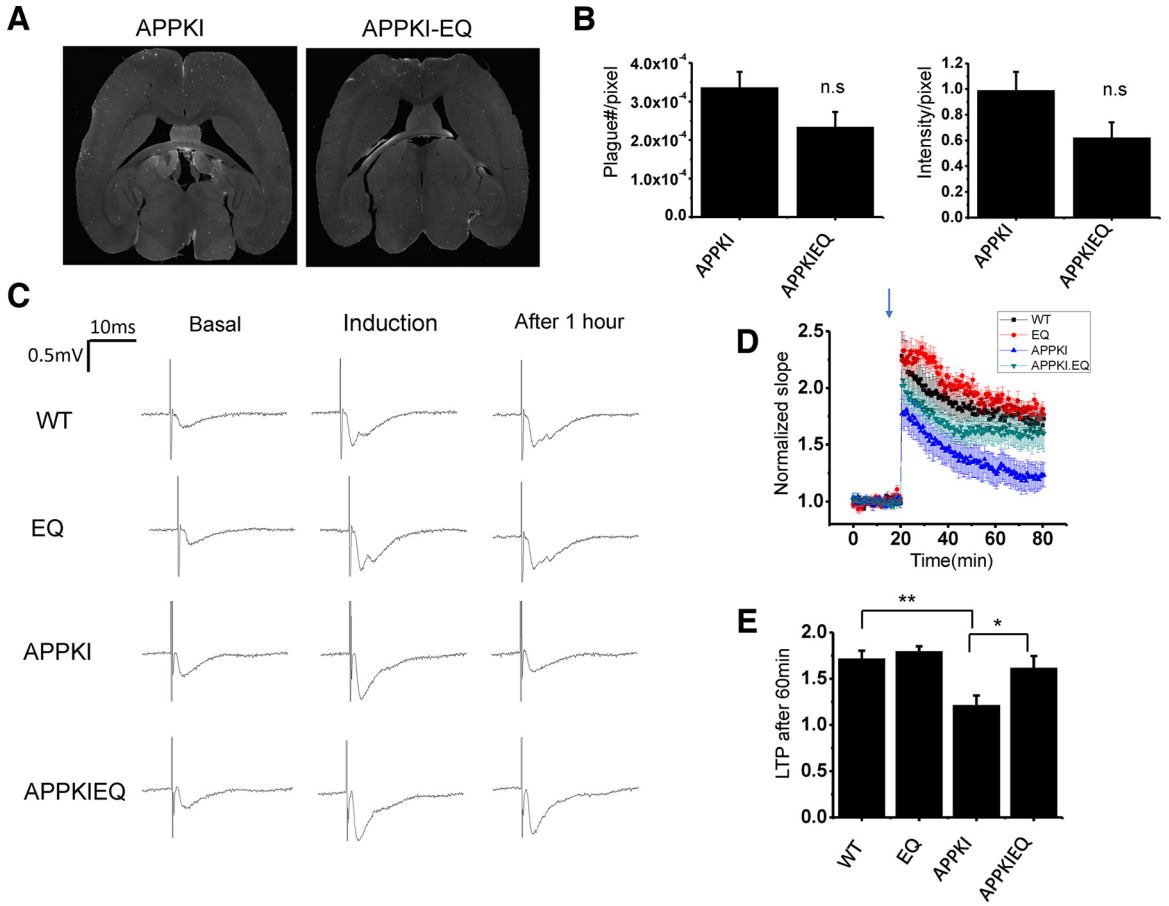

Figure 7. RyanR2-E4872Q (EQ) mutation rescues LTP defect in APPKI mice. ***A***, Representative IsoCyte laser-scanning images of horizontal brain slices from 13-month-old APPKI and APPKI;EQ mice stained with fluorescently labeled 6E10 antiamyloid antibodies. ***B***, Average density of amyloid plaques and average signal intensity within the plaques for APPKI and APPKI;EQ mouse samples. The data are shown as the mean ± SE ($n \geq 6$ mice). n.s., Nonsignificant, Student's *t* test. ***C***, Sample fEPSP traces are shown for 6-month-old WT, EQ, APPKI, and APPKI:EQ brain slices before stimulation (basal), immediately after tetanus stimulation (induction), and 1 h after tetanus stimulation (after 1 h). ***D***, Normalized and averaged slope of fEPSP recorded from 6-month-old hippocampal slices from wild-type, EQ, APPKI, and APPKI;EQ mice. The LTP was induced by HFS, as shown by the arrow. ***E***, Averaged change in normalized fEPSP slope recorded 1 h after HFS for wild-type, EQ, APPKI, and APPKI;EQ mice. The data are shown as the mean ± SE ($n \geq 8$ mice). *$p < 0.05$, **$p < 0.01$, one-way ANOVA with Tukey's *post hoc* test. Note: WT and EQ data were the same as in Figure 6.

and neurofibrillary tangles (formed by hyperphosphorylated tau protein). Despite extensive research, the molecular basis underlying AD pathogenesis is still not fully understood, and there are no effective treatments to block or reverse AD progression. Autophagy plays an important role in clearing damaged organelles and long-lived protein aggregates and neuronal cells depend heavily on autophagy to clear large and insoluble protein aggregates to maintain protein homeostasis (Malampati et al., 2020). Accumulating evidence indicates that impaired autophagy contributes to AD pathogenesis (Liu and Li, 2019; Kuang et al., 2020; Chen et al., 2021; Zhang et al., 2021; Mustaly-Kalimi and Stutzmann, 2022). For example, it has been suggested that FAD mutations in presenilins may impair autophagy through defective lysosomal acidification or reduced lysosomal Ca^{2+} content (Lee et al., 2010, 2015; Coen et al., 2012; Fedeli et al., 2019; for review, see Bezprozvanny, 2012). There is also a growing body of evidence that dysregulation in neuronal Ca^{2+} signaling plays a major role in the initiation of AD pathogenesis (Bezprozvanny and Mattson, 2008; Popugaeva et al., 2015; Briggs et al., 2017). RyanR-mediated Ca^{2+} signaling is upregulated in early-stage AD patients and FAD mouse models (Kelliher et al., 1999; Stutzmann et al., 2006; Supnet et al., 2006; Zhang et al., 2010; Bruno et al., 2012). Previous reports demonstrated that genetic or pharmacological inhibition of RyanR activity in AD mouse models resulted in beneficial effects, such as improved synaptic plasticity and the normalization of behavioral and cognitive functions with or without reduced amyloid load (Chakroborty et al., 2012; Oulès et al., 2012; Peng et al., 2012). Possible connections between neuronal Ca^{2+} dysregulation and autophagy in AD has been proposed (Filadi and Pizzo, 2019). It has been suggested that the upregulation of RyanR expression and activity may lead to the dysregulation of autophagy (Vervliet et al., 2017; McDaid et al., 2020), but no experimental evidence was provided in support of this hypothesis.

In the present study, we took advantage of the RyanR2-E4872Q KI mouse model (EQ) in which RyanR2 activity is reduced because of shortened channel open time (Chen et al., 2014). Use of this model enabled us to evaluate the consequences of the reduction of endogenous RyanR2 activity in neuronal cells for autophagy and for AD-related phenotypes. Based on the obtained results, we propose a model that directly links basal activity of RyanR2 to neuronal autophagy (Fig. 8*A*). In this model, we propose that basal Ca^{2+} activity of RyanR2 in neuronal cells leads to continuous activation of CaN, which in turn inhibits the AMPK–ULK1 pathway that regulates the autophagic flux. In EQ neurons, the reduction of RyanR2 activity because of the EQ

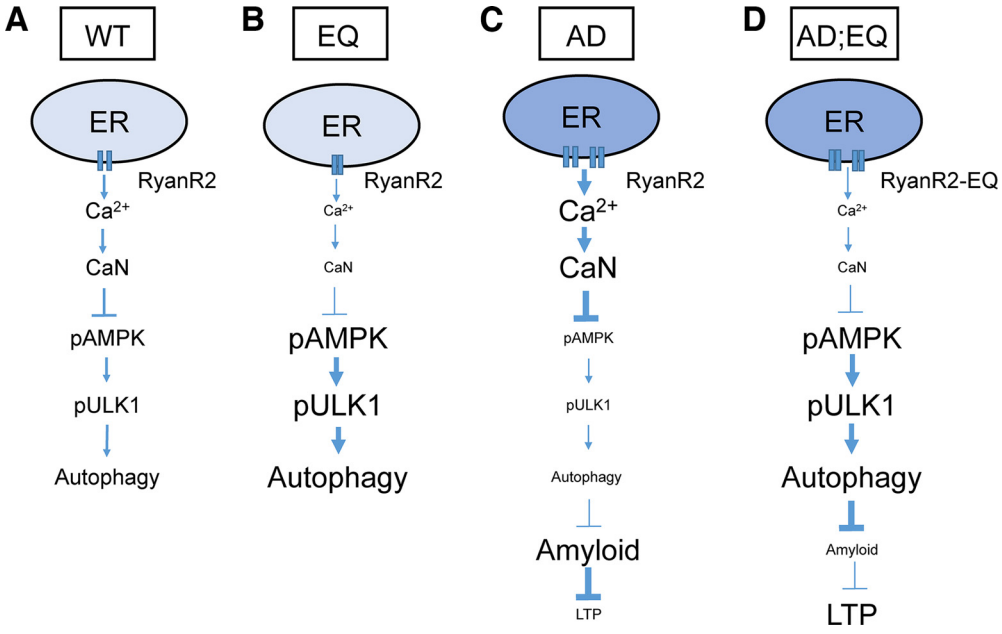

Figure 8. RyanR2-mediated basal calcium flux and control of neuronal autophagy in health and disease. ***A***, Wild-type. Basal Ca^{2+} flux from ER via RyanR2 maintains the steady-state level of CaN activation in neuronal cytoplasm. CaN dephosphorylates and inactivates AMPK, reducing the levels of ULK1 phosphorylation (Ser555) and limiting autophagic flux. ***B***, EQ mutant. Basal Ca^{2+} flux from ER via RyanR2 is reduced because of E4872Q gating mutation and shortened channel open times. Reduction of basal Ca^{2+} flux from the ER leads to reduced steady-state levels of CaN activity, increase in AMPK and ULK1 (Ser555) phosphorylation, and stimulation of autophagic flux. ***C***, AD. Basal Ca^{2+} flux from ER is enhanced in early AD and aging because of overloaded ER Ca^{2+} stores and increased the levels of RyanR2 expression. Resulting enhancement of basal Ca^{2+} flux leads to overstimulation of CaN, reduced levels of AMPK and ULK1 (Ser555) phosphorylation, and reduced autophagic flux. Reduced autophagy impaired the clearance of APP and APP fragments, causing accumulation of Aβ oligomers and plaques and impaired synaptic plasticity (LTP). ***D***, AD;EQ. Basal Ca^{2+} from ER is normalized in AD;EQ mutants because of reduced RyanR2 channel open times. As a result, steady-state CaN activity is also normalized, causing increased phosphorylation of AMPK and ULK1 (Ser555) and disinhibition of autophagy. Enhanced autophagy promotes the clearance of APP and APP fragments, reduces the amounts of Aβ oligomers and amyloid plaques, leading to the rescue of synaptic plasticity (LTP) defects.

mutation leads to reduced activity of CaN and disinhibition of the AMPK–ULK1 pathway, resulting in enhanced autophagic flux (Fig. 8*B*). Similar effects are achieved as a result of RyanR inhibition by ryanodine (Figs. 2, 3). The proposed model is also supported by our results with specific CaN inhibitor FK506, that resulted in the activation of AMPK and ULK1 and a dramatic upregulation of neuronal autophagy (Figs. 2, 3). Our model of control of neuronal autophagy by RyanR2 and Ca^{2+} (Fig. 8*A*) is similar to the model that was proposed previously in cardiomyocytes (He et al., 2014). It should be noted that cytosolic Ca^{2+} signals may also trigger autophagy. For example, it has been reported that the activation of RyanR may induce autophagy-dependent cell death by stimulating the CaMKK2–AMPK–mTOR signaling pathway (Chung et al., 2016; Law et al., 2019). To reconcile these results with our conclusions, we propose that low levels of basal Ca^{2+} flux because of spontaneous activity of RyanR2 primarily stimulate CaN and inhibit autophagy, but high levels of Ca^{2+} during evoked Ca^{2+} release lead to the activation of CaMKK2, which promotes autophagy. Both CaN and CaMKK2 are regulated by Ca^{2+}/calmodulin, and differential modulation of CaN and CaMKII by low and high Ca^{2+} elevations has already been described (Saucerman and Bers, 2008; Stefan et al., 2008).

We further propose that overactivation of RyanR2 and Ca^{2+} release from ER contributes to impaired autophagy in early AD (Fig. 8*C*). Specifically, we reasoned that overloaded ER Ca^{2+} stores and/or increased expression of RyanR2 leads to increased basal Ca^{2+} flux and overactivation of CaN. Overactivation of CaN leads to further suppression of the AMPK–ULK1 pathway and reduced autophagy. In turn, reduced autophagy impairs the clearance of APP and APP proteolytic fragments, eventually leading to the accumulation of soluble Aβ42 oligomers, amyloid plaques, and impaired synaptic plasticity. This model is supported by the observation of reduced autophagic flux and reduced pAMPK/AMPK levels in APPKI neurons (Figs. 1, 3). Based on this hypothesis, we can explain the beneficial effects of the RyanR2 EQ mutation in AD models (Fig. 8*D*). We propose that the reduction of Ca^{2+} flux from ER in AD;EQ neurons normalizes CaN activity and causes disinhibition of the AMPK–ULK1 pathway and stimulation of autophagy. This idea is supported by our observation of autophagic flux rescue in APPKI neurons in the presence of the EQ mutation or following pharmacological inhibition of RyanR with ryanodine or inhibition of CaN with FK506 (Figs. 1-4). It is also supported by the rescue of autophagy in the APPPS1;EQ mouse model (Fig. 4). We further propose that increased autophagy leads to enhanced clearance of APP and APP fragments, reduction in the levels of soluble Aβ42 oligomers and amyloid plaques, and rescue of LTP defects. This idea is supported by the observation of reduced APP and APP-CTF levels and reduced amounts of Aβ40 and Aβ42 in culture media of APPKI;EQ neurons (Fig. 5); reduced plaque load and reduced Aβ40 and Aβ42 concentrations in cortex homogenates in APPPS1;EQ mice (Fig. 6); and rescue of LTP defects in both APPKI;EQ and APPPS1;EQ mice (Figs. 6, 7). Interestingly, previous studies suggested beneficial effects of CaN inhibition in multiple models of AD (Dineley et al., 2007, 2010; Taglialatela et al., 2009; Wu et al., 2010; D'Amelio et al., 2011; Rozkalne et al., 2011; Kim et al., 2015; Stallings et al., 2018). Moreover, *post hoc* analysis of epidemiological data revealed that the incidence of AD was significantly reduced in transplant patients chronically treated with FK-506 (Taglialatela et al., 2015). It is possible that some of

these beneficial effects observed with FK506 and other CaN inhibitors in AD are also related to stimulation of neuronal autophagy as our model suggests (Fig. 8).

Comparison of results obtained with APPKI and APPS1 mice enabled us to compare effects on autophagy before and after amyloidosis. At 6 months of age, the levels of LC3-positive autophagosomes were upregulated in APPPS1 mouse brains but not in APPKI mouse brains (Fig. 4). However, both APPPS1 and APPKI mouse brains displayed decreased LAMP1-positive lysosomal puncta and decreased autolysosome at the same age (Fig. 4). Since APPPS1 mice, but not APPPKI mice, display amyloid plaques at this age, our results suggest that impaired autophagy-lysosomal function is an early event (before plaque formation) in the AD pathogenesis pathway, and that ER Ca^{2+} overload and upregulation of RyanR2 activity in early AD may contribute to these problems. We propose that the upregulation of autophagosome formation is more likely to be a late-stage compensatory mechanism induced in response to amyloid plaque burden. Our results suggest that the upregulation of autophagosome formation in APPPS1 mice is not enough to rescue neurons from damage, but the EQ mutation disinhibits the autophagic flux defect and leads to a rescue effect in APPS1;EQ mice. This conclusion is consistent with previous and recent reports (Lauritzen et al., 2016; Long et al., 2020; Lee et al., 2022). It is also consistent with the idea that autophagy is constitutively active and highly efficient in healthy neurons (Fig. 1) and that the autophagic pathology observed in late AD most likely arises from impaired clearance of autophagic vacuoles (AVs) rather than from strong autophagy induction (Boland et al., 2008). Additionally, AMPK–ULK1 pathways were also important for mitophagy regulation (Fang et al., 2019); impaired mitophagy is also important for AD pathogenesis (Ye et al., 2015; Vaillant-Beuchot et al., 2021; Mary et al., 2023), so overactivation of the RyanR-mediated CaN–AMPK–ULK1 pathway may also be abnormal and involved in mitophagy in AD.

It should also be noted that previous studies also demonstrated the benefit of crossing EQ mice with 5XFAD or 3xTg-AD mouse models of AD (Yao et al., 2020; Liu et al., 2021; Sun et al., 2021). These authors observed improved synaptic plasticity and rescue of cognitive functions without significant changes in amyloid load. This is in contrast to our studies performed with APPPS1 and APPKI mice. It is possible that the amyloid load in 5xFAD mice is very large and upregulation of autophagic pathway may not be sufficient to significantly reduce it. It is also possible that reduced activity of RyanR2 exerts multiple beneficial effects in addition to the upregulation of autophagy. CaN has many other downstream targets, for example, the pCREB pathway, which is also important for synaptic plasticity and has been implicated in memory impairment in AD (Saura and Valero, 2011; Amidfar et al., 2020). In our studies, we found in APPKI;EQ hippocampal cultures pCREB/CREB was significantly increased compared with APPKI cultures (data not shown), suggesting that this pathway may also play some role in the rescue effects in APPKI;EQ mice. In addition to the CaN signaling pathway, it also has been suggested that the inhibition of RyanR2 may lead to the rescue of AD-associated neuronal hyperexcitability (Yao et al., 2020; Liu et al., 2021; Sun et al., 2021), reduction in ER stress (Nakamura et al., 2021), and direct effects on β-secretase and γ-secretase activities and APP phosphorylation (Oulès et al., 2012). The model proposed here (Fig. 8*D*) provides a novel potential explanation for the benefits of pharmacological inhibition of RyanR in AD and may also provide an additional target for therapeutic intervention in AD.

References

Al-Bari MAA, Xu PY (2020) Molecular regulation of autophagy machinery by mTOR-dependent and -independent pathways. Ann N Y Acad Sci 1467:3–20.

Amidfar M, de Oliveira J, Kucharska E, Budni J, Kim YK (2020) The role of CREB and BDNF in neurobiology and treatment of Alzheimer's disease. Life Sci 257:118020.

Bezprozvanny I (2012) Presenilins: a novel link between intracellular calcium signaling and lysosomal function? J Cell Biol 198:7–10.

Bezprozvanny I, Mattson MP (2008) Neuronal calcium mishandling and the pathogenesis of Alzheimer's disease. Trends Neurosci 31:454–463.

Boland B, Kumar A, Lee S, Platt FM, Wegiel J, Yu WH, Nixon RA (2008) Autophagy induction and autophagosome clearance in neurons: relationship to autophagic pathology in Alzheimer's disease. J Neurosci 28:6926–6937.

Braak H, Braak E (1991) Neuropathological stageing of Alzheimer-related changes. Acta Neuropathol 82:239–259.

Braak H, Del Tredici K (2015) The preclinical phase of the pathological process underlying sporadic Alzheimer's disease. Brain 138:2814–2833.

Briggs CA, Chakroborty S, Stutzmann GE (2017) Emerging pathways driving early synaptic pathology in Alzheimer's disease. Biochem Biophys Res Commun 483:988–997.

Bruno AM, Huang JY, Bennett DA, Marr RA, Hastings ML, Stutzmann GE (2012) Altered ryanodine receptor expression in mild cognitive impairment and Alzheimer's disease. Neurobiol Aging 33:e1001.e1–1001.e6.

Buzsáki G, Moser EI (2013) Memory, navigation and theta rhythm in the hippocampal-entorhinal system. Nat Neurosci 16:130–138.

Cárdenas C, Miller RA, Smith I, Bui T, Molgó J, Müller M, Vais H, Cheung KH, Yang J, Parker I, Thompson CB, Birnbaum MJ, Hallows KR, Foskett JK (2010) Essential regulation of cell bioenergetics by constitutive InsP3 receptor Ca2+ transfer to mitochondria. Cell 142:270–283.

Cataldo AM, Peterhoff CM, Schmidt SD, Terio NB, Duff K, Beard M, Mathews PM, Nixon RA (2004) Presenilin mutations in familial Alzheimer disease and transgenic mouse models accelerate neuronal lysosomal pathology. J Neuropathol Exp Neurol 63:821–830.

Chakroborty S, Goussakov I, Miller MB, Stutzmann GE (2009) Deviant ryanodine receptor-mediated calcium release resets synaptic homeostasis in presymptomatic 3xTg-AD mice. J Neurosci 29:9458–9470.

Chakroborty S, Briggs C, Miller MB, Goussakov I, Schneider C, Kim J, Wicks J, Richardson JC, Conklin V, Cameransi BG, Stutzmann GE (2012) Stabilizing ER Ca2+ channel function as an early preventative strategy for Alzheimer's disease. PLoS One 7:e52056.

Chen J, He HJ, Ye QQ, Feng FF, Wang WW, Gu YY, Han RY, Xie CL (2021) Defective autophagy and mitophagy in Alzheimer's disease: mechanisms and translational implications. Mol Neurobiol 58:5289–5302.

Chen WQ, et al. (2014) The ryanodine receptor store-sensing gate controls Ca2+ waves and Ca2+-triggered arrhythmias. Nat Med 20:184–192.

Chung KM, Jeong EJ, Park H, An HK, Yu SW (2016) Mediation of autophagic cell death by type 3 ryanodine receptor (RyR3) in adult hippocampal neural stem cells. Front Cell Neurosci 10:116.

Coen K, Flannagan RS, Baron S, Carraro-Lacroix LR, Wang D, Vermeire W, Michiels C, Munck S, Baert V, Sugita S, Wuytack F, Hiesinger PR, Grinstein S, Annaert W (2012) Lysosomal calcium homeostasis defects, not proton pump defects, cause endo-lysosomal dysfunction in PSEN-deficient cells. J Cell Biol 198:23–35.

Colino A, Malenka RC (1993) Mechanisms underlying induction of long-term potentiation in rat medial and lateral perforant paths in vitro. J Neurophysiol 69:1150–1159.

D'Amelio M, Cavallucci V, Middei S, Marchetti C, Pacioni S, Ferri A, Diamantini A, De Zio D, Carrara P, Battistini L, Moreno S, Bacci A, Ammassari-Teule M, Marie H, Cecconi F (2011) Caspase-3 triggers early synaptic dysfunction in a mouse model of Alzheimer's disease. Nat Neurosci 14:69–76.

Decuypere JP, Bultynck G, Parys JB (2011a) A dual role for Ca(2+) in autophagy regulation. Cell Calcium 50:242–250.

Decuypere JP, Welkenhuyzen K, Luyten T, Ponsaerts R, Dewaele M, Molgo J, Agostinis P, Missiaen L, De Smedt H, Parys JB, Bultynck G (2011b) Ins (1,4,5)P3 receptor-mediated Ca2+ signaling and autophagy induction are interrelated. Autophagy 7:1472–1489.

Dineley KT, Hogan D, Zhang WR, Taglialatela G (2007) Acute inhibition of calcineurin restores associative learning and memory in Tg2576 APP transgenic mice. Neurobiol Learn Mem 88:217–224.

Dineley KT, Kayed R, Neugebauer V, Fu Y, Zhang W, Reese LC, Taglialatela G (2010) Amyloid-beta oligomers impair fear conditioned memory in a calcineurin-dependent fashion in mice. J Neurosci Res 88:2923–2932.

Egan DF, Shackelford DB, Mihaylova MM, Gelino S, Kohnz RA, Mair W, Vasquez DS, Joshi A, Gwinn DM, Taylor R, Asara JM, Fitzpatrick J, Dillin A, Viollet B, Kundu M, Hansen M, Shaw RJ (2011) Phosphorylation of ULK1 (hATG1) by AMP-activated protein kinase connects energy sensing to mitophagy. Science 331:456–461.

Evrard C, Kienlen-Campard P, Coevoet M, Opsomer R, Tasiaux B, Melnyk P, Octave JN, Buée L, Sergeant N, Vingtdeux V (2018) Contribution of the endosomal-lysosomal and proteasomal systems in amyloid-β precursor protein derived fragments processing. Front Cell Neurosci 12:435.

Fang EF, Hou Y, Palikaras K, Adriaanse BA, Kerr JS, Yang B, Lautrup S, Hasan-Olive MM, Caponio D, Dan X, Rocktäschel P, Croteau DL, Akbari M, Greig NH, Fladby T, Nilsen H, Cader MZ, Mattson MP, Tavernarakis N, Bohr VA (2019) Mitophagy inhibits amyloid-β and tau pathology and reverses cognitive deficits in models of Alzheimer's disease. Nat Neurosci 22:401–412.

Fedeli C, Filadi R, Rossi A, Mammucari C, Pizzo P (2019) PSEN2 (presenilin 2) mutants linked to familial Alzheimer disease impair autophagy by altering Ca2+ homeostasis. Autophagy 15:2044–2062.

Filadi R, Pizzo P (2019) Defective autophagy and Alzheimer's disease: is calcium the key? Neural Regen Res 14:2081–2082.

Furuichi T, Furutama D, Hakamata Y, Nakai J, Takeshima H, Mikoshiba K (1994) Multiple types of ryanodine receptor/Ca^{2+} release channels are differentially expressed in rabbit brain. J Neurosci 14:4794–4805.

Giannini G, Conti A, Mammarella S, Scrobogna M, Sorrentino V (1995) The ryanodine receptor/calcium channel genes are widely and differentially expressed in murine brain and peripheral tissues. J Cell Biol 128:893–904.

Haass C, Capell A, Citron M, Teplow DB, Selkoe DJ (1995) The vacuolar H (+)-ATPase inhibitor bafilomycin A1 differentially affects proteolytic processing of mutant and wild-type beta-amyloid precursor protein. J Biol Chem 270:6186–6192.

He H, Liu X, Lv L, Liang H, Leng B, Zhao D, Zhang Y, Du Z, Chen X, Li S, Lu Y, Shan H (2014) Calcineurin suppresses AMPK-dependent cytoprotective autophagy in cardiomyocytes under oxidative stress. Cell Death Dis 5:e997.

Kelliher M, Fastbom J, Cowburn RF, Bonkale W, Ohm TG, Ravid R, Sorrentino V, O'Neill C (1999) Alterations in the ryanodine receptor calcium release channel correlate with Alzheimer's disease neurofibrillary and beta-amyloid pathologies. Neuroscience 92:499–513.

Khan MT, Joseph SK (2010) Role of inositol trisphosphate receptors in autophagy in DT40 cells. J Biol Chem 285:16912–16920.

Kim S, Violette CJ, Ziff EB (2015) Reduction of increased calcineurin activity rescues impaired homeostatic synaptic plasticity in presenilin 1 M146V mutant. Neurobiol Aging 36:3239–3246.

Klionsky DJ, et al (2021) Guidelines for the use and interpretation of assays for monitoring autophagy (4th edition). Autophagy 17:1–382.

Kuang H, Tan CY, Tian HZ, Liu LH, Yang MW, Hong FF, Yang SL (2020) Exploring the bi-directional relationship between autophagy and Alzheimer's disease. Cns Neurosci Ther 26:155–166.

Lacampagne A, Liu XP, Reiken S, Bussiere R, Meli AC, Lauritzen I, Teich AF, Zalk R, Saint N, Arancio O, Bauer C, Duprat F, Briggs CA, Chakroborty S, Stutzmann GE, Shelanski ML, Checler F, Chami M, Marks AR (2017) Post-translational remodeling of ryanodine receptor induces calcium leak leading to Alzheimer's disease-like pathologies and cognitive deficits. Acta Neuropathol 134:749–767.

Lam D, Kosta A, Luciani MF, Golstein P (2008) The inositol 1,4,5-trisphosphate receptor is required to signal autophagic cell death. Mol Biol Cell 19:691–700.

Lauritzen I, Pardossi-Piquard R, Bourgeois A, Pagnotta S, Biferi MG, Barkats M, Lacor P, Klein W, Bauer C, Checler F (2016) Intraneuronal aggregation of the β-CTF fragment of APP (C99) induces Aβ-independent lysosomal-autophagic pathology. Acta Neuropathol 132:257–276.

Law BYK, Michelangeli F, Qu YQ, Xu SW, Han Y, Mok SWFA, Dias IRDR, Javed MU, Chan WK, Xue WW, Yao X-J, Zeng W, Zhang H, Wang J-R, Liu L, Wong VKW (2019) Neferine induces autophagy-dependent cell death in apoptosis-resistant cancers via ryanodine receptor and Ca2+-dependent mechanism. Sci Rep 9:20034.

Lee JH, Yu WH, Kumar A, Lee S, Mohan PS, Peterhoff CM, Wolfe DM, Martinez-Vicente M, Massey AC, Sovak G, Uchiyama Y, Westaway D, Cuervo AM, Nixon RA (2010) Lysosomal proteolysis and autophagy require presenilin 1 and are disrupted by Alzheimer-related PS1 mutations. Cell 141:1146–1158.

Lee JH, McBrayer MK, Wolfe DM, Haslett LJ, Kumar A, Sato Y, Lie PP, Mohan P, Coffey EE, Kompella U, Mitchell CH, Lloyd-Evans E, Nixon RA (2015) Presenilin 1 maintains lysosomal Ca(2+) homeostasis via TRPML1 by regulating vATPase-mediated lysosome acidification. Cell Rep 12:1430–1444.

Lee JH, Yang DS, Goulbourne CN, Im E, Stavrides P, Pensalfini A, Chan H, Bouchet-Marquis C, Bleiwas C, Berg MJ, Huo C, Peddy J, Pawlik M, Levy E, Rao M, Staufenbiel M, Nixon RA (2022) Faulty autolysosome acidification in Alzheimer's disease mouse models induces autophagic build-up of Aβ in neurons, yielding senile plaques. Nat Neurosci 25:688–701.

Leeman DS, Hebestreit K, Ruetz T, Webb AE, McKay A, Pollina EA, Dulken BW, Zhao X, Yeo RW, Ho TT, Mahmoudi S, Devarajan K, Passegué E, Rando TA, Frydman J, Brunet A (2018) Lysosome activation clears aggregates and enhances quiescent neural stem cell activation during aging. Science 359:1277–1283.

Liu J, Li L (2019) Targeting autophagy for the treatment of Alzheimer's disease: challenges and opportunities. Front Mol Neurosci 12:203.

Liu J, Supnet C, Sun S, Zhang H, Good L, Popugaeva E, Bezprozvanny I (2014) The role of ryanodine receptor type 3 in a mouse model of Alzheimer disease. Channels (Austin) 8:230–242.

Liu Y, Yao J, Song Z, Guo W, Sun B, Wei J, Estillore JP, Back TG, Chen SRW (2021) Limiting RyR2 open time prevents Alzheimer's disease-related deficits in the 3xTG-AD mouse model. J Neurosci Res 99:2906–2921.

Long Z, Chen J, Zhao Y, Zhou W, Yao Q, Wang Y, He G (2020) Dynamic changes of autophagic flux induced by Abeta in the brain of postmortem Alzheimer's disease patients, animal models and cell models. Aging (Albany NY) 12:10912–10930.

Lu Y, Akinwumi BC, Shao Z, Anderson HD (2014) Ligand activation of cannabinoid receptors attenuates hypertrophy of neonatal rat cardiomyocytes. J Cardiovasc Pharmacol 64:420–430.

Malampati S, Song JX, Tong BCK, Nalluri A, Yang CB, Wang ZY, Sreenivasmurthy SG, Zhu Z, Liu J, Su CF, Krishnamoorthi S, Iyaswamy A, Cheung K-H, Lu J-H, Li M (2020) Targeting aggrephagy for the treatment of Alzheimer's disease. Cells 9:311.

Mary A, Eysert F, Checler F, Chami M (2023) Mitophagy in Alzheimer's disease: molecular defects and therapeutic approaches. Mol Psychiatry 28:202–216.

McDaid J, Mustaly-Kalimi S, Stutzmann GE (2020) Ca^{2+} dyshomeostasis disrupts neuronal and synaptic function in Alzheimer's disease. Cells 9:2655.

Medina DL, Di Paola S, Peluso I, Armani A, De Stefani D, Venditti R, Montefusco S, Scotto-Rosato A, Prezioso C, Forrester A, Settembre C, Wang W, Gao Q, Xu H, Sandri M, Rizzuto R, De Matteis MA, Ballabio A (2015) Lysosomal calcium signalling regulates autophagy through calcineurin and TFEB. Nat Cell Biol 17:288–299.

Mustaly-Kalimi S, Stutzmann GE (2022) Protein mishandling and impaired lysosomal proteolysis generated through calcium dysregulation in Alzheimer's disease. Proc Natl Acad Sci U S A 119:e2211999119.

Nakamura Y, Yamamoto T, Xu XJ, Kobayashi S, Tanaka S, Tamitani M, Saito T, Saido TC, Yano M (2021) Enhancing calmodulin binding to ryanodine receptor is crucial to limit neuronal cell loss in Alzheimer disease. Sci Rep 11:7289.

Nixon RA, Wegiel J, Kumar A, Yu WH, Peterhoff C, Cataldo A, Cuervo AM (2005) Extensive involvement of autophagy in Alzheimer disease: an immuno-electron microscopy study. J Neuropathol Exp Neurol 64:113–122.

Oulès B, Del Prete D, Greco B, Zhang X, Lauritzen I, Sevalle J, Moreno S, Paterlini-Bréchot P, Trebak M, Checler F, Benfenati F, Chami M (2012) Ryanodine receptor blockade reduces amyloid-β load and memory impairments in Tg2576 mouse model of Alzheimer disease. J Neurosci 32:11820–11834.

Peng J, Liang G, Inan S, Wu Z, Joseph DJ, Meng QC, Peng Y, Eckenhoff MF, Wei HF (2012) Dantrolene ameliorates cognitive decline and neuropathology in Alzheimer triple transgenic mice. Neurosci Lett 516:274–279.

Popugaeva E, Vlasova OL, Bezprozvanny I (2015) Restoring calcium homeostasis to treat Alzheimer's disease: a future perspective. Neurodegener Dis Manag 5:395–398.

Qiao H, Li Y, Xu ZD, Li WX, Fu ZJ, Wang YZ, King A, Wei HF (2017) Propofol affects neurodegeneration and neurogenesis by regulation of

autophagy via effects on intracellular calcium homeostasis. Anesthesiology 127:490–501.
Radde R, Bolmont T, Kaeser SA, Coomaraswamy J, Lindau D, Stoltze L, Calhoun ME, Jäggi F, Wolburg H, Gengler S, Haass C, Ghetti B, Czech C, Hölscher C, Mathews PM, Jucker M (2006) Abeta42-driven cerebral amyloidosis in transgenic mice reveals early and robust pathology. EMBO Rep 7:940–946.
Rahman MA, Rahman MS, Rahman MH, Rasheduzzaman M, Mamun-Or-Rashid ANM, Uddin MJ, Rahman MR, Hwang H, Pang MG, Rhim H (2021) Modulatory effects of autophagy on APP processing as a potential treatment target for Alzheimer's disease. Biomedicines 9:5.
Rozkalne A, Hyman BT, Spires-Jones TL (2011) Calcineurin inhibition with FK506 ameliorates dendritic spine density deficits in plaque-bearing Alzheimer model mice. Neurobiol Dis 41:650–654.
Rubinsztein DC, Cuervo AM, Ravikumar B, Sarkar S, Korolchuk V, Kaushik S, Klionsky DJ (2009) In search of an "autophagomometer". Autophagy 5:585–589.
Saito T, Matsuba Y, Mihira N, Takano J, Nilsson P, Itohara S, Iwata N, Saido TC (2014) Single App knock-in mouse models of Alzheimer's disease. Nat Neurosci 17:661–663.
Sanchez-Varo R, Trujillo-Estrada L, Sanchez-Mejias E, Torres M, Baglietto-Vargas D, Moreno-Gonzalez I, De Castro V, Jimenez S, Ruano D, Vizuete M, Davila JC, Garcia-Verdugo JM, Jimenez AJ, Vitorica J, Gutierrez A (2012) Abnormal accumulation of autophagic vesicles correlates with axonal and synaptic pathology in young Alzheimer's mice hippocampus. Acta Neuropathol 123:53–70.
Sardiello M, Palmieri M, di Ronza A, Medina DL, Valenza M, Gennarino VA, Di Malta C, Donaudy F, Embrione V, Polishchuk RS, Banfi S, Parenti G, Cattaneo E, Ballabi A (2009) A gene network regulating lysosomal biogenesis and function. Science 325:473–477.
Saucerman JJ, Bers DM (2008) Calmodulin mediates differential sensitivity of CaMKII and calcineurin to local Ca2+ in cardiac myocytes. Biophys J 95:4597–4612.
Saura CA, Valero J (2011) The role of CREB signaling in Alzheimer's disease and other cognitive disorders. Rev Neurosci 22:153–169.
Settembre C, Zoncu R, Medina DL, Vetrini F, Erdin S, Erdin S, Huynh T, Ferron M, Karsenty G, Vellard MC, Facchinetti V, Sabatini DM, Ballabio A (2012) A lysosome-to-nucleus signalling mechanism senses and regulates the lysosome via mTOR and TFEB. EMBO J 31:1095–1108.
Smith IF, Hitt B, Green KN, Oddo S, LaFerla FM (2005) Enhanced caffeine-induced Ca2+ release in the 3xTg-AD mouse model of Alzheimer's disease. J Neurochem 94:1711–1718.
Stallings NR, O'Neal MA, Hu J, Kavalali ET, Bezprozvanny I, Malter JS (2018) Pin1 mediates $A\beta_{42}$-induced dendritic spine loss. Sci Signal 11: aap8734.
Stefan MI, Edelstein SJ, Le Novère N (2008) An allosteric model of calmodulin explains differential activation of PP2B and CaMKII. Proc Natl Acad Sci U S A 105:10768–10773.
Stutzmann GE, Smith I, Caccamo A, Oddo S, Laferla FM, Parker I (2006) Enhanced ryanodine receptor recruitment contributes to Ca^{2+} disruptions in young, adult, and aged Alzheimer's disease mice. J Neurosci 26:5180–5189.
Suire CN, Abdul-Hay SO, Sahara T, Kang D, Brizuela MK, Saftig P, Dickson DW, Rosenberry TL, Leissring MA (2020) Cathepsin D regulates cerebral $A\beta$42/40 ratios via differential degradation of $A\beta$42 and $A\beta$40. Alzheimers Res Ther 12:80.
Sukumaran P, Da Conceicao VN, Sun YY, Ahamad N, Saraiva LR, Selvaraj S, Singh BB (2021) Calcium signaling regulates autophagy and apoptosis. Cells 10:2125.
Sun B, Yao J, Chen AW, Estillore JP, Wang R, Back TG, Chen SRW (2021) Genetically and pharmacologically limiting RyR2 open time prevents neuronal hyperactivity of hippocampal CA1 neurons in brain slices of 5xFAD mice. Neurosci Lett 758:136011.
Supnet C, Grant J, Kong H, Westaway D, Mayne M (2006) Amyloid-beta-(1-42) increases ryanodine receptor-3 expression and function in neurons of TgCRND8 mice. J Biol Chem 281:38440–38447.
Taglialatela G, Hogan D, Zhang WR, Dineley KT (2009) Intermediate- and long-term recognition memory deficits in Tg2576 mice are reversed with acute calcineurin inhibition. Behav Brain Res 200:95–99.
Taglialatela G, Rastellini C, Cicalese L (2015) Reduced incidence of dementia in solid organ transplant patients treated with calcineurin inhibitors. J Alzheimers Dis 47:329–333.
Vaillant-Beuchot L, et al. (2021) Accumulation of amyloid precursor protein C-terminal fragments triggers mitochondrial structure, function, and mitophagy defects in Alzheimer's disease models and human brains. Acta Neuropathol 141:39–65.
Valladares D, Utreras-Mendoza Y, Campos C, Morales C, Diaz-Vegas A, Contreras-Ferrat A, Westermeier F, Jaimovich E, Marchi S, Pinton P, Lavandero S (2018) IP3 receptor blockade restores autophagy and mitochondrial function in skeletal muscle fibers of dystrophic mice. Biochim Biophys Acta Mol Basis Dis 1864:3685–3695.
Vervliet T (2018) Ryanodine receptors in autophagy: implications for neurodegenerative diseases? Front Cell Neurosci 12:89.
Vervliet T, Pintelon I, Welkenhuyzen K, Bootman MD, Bannai H, Mikoshiba K, Martinet W, Kasri NN, Parys JB, Bultynck G (2017) Basal ryanodine receptor activity suppresses autophagic flux. Biochem Pharmacol 132:133–142.
Vingtdeux V, Hamdane M, Bégard S, Loyens A, Delacourte A, Beauvillain JC, Buée L, Marambaud P, Sergeant N (2007) Intracellular pH regulates amyloid precursor protein intracellular domain accumulation. Neurobiol Dis 25:686–696.
Wu HY, Hudry E, Hashimoto T, Kuchibhotla K, Rozkalne A, Fan Z, Spires-Jones T, Xie H, Arbel-Ornath M, Grosskreutz CL, Bacskai BJ, Hyman BT (2010) Amyloid β induces the morphological neurodegenerative triad of spine loss, dendritic simplification, and neuritic dystrophies through calcineurin activation. J Neurosci 30:2636–2649.
Yang DS, Stavrides P, Mohan PS, Kaushik S, Kumar A, Ohno M, Schmidt SD, Wesson D, Bandyopadhyay U, Jiang Y, Pawlik M, Peterhoff CM, Yang AJ, Wilson DA, St George-Hyslop P, Westaway D, Mathews PM, Levy E, Cuervo AM, Nixon RA (2011) Reversal of autophagy dysfunction in the TgCRND8 mouse model of Alzheimer's disease ameliorates amyloid pathologies and memory deficits. Brain 134:258–277.
Yao J, Sun B, Institoris A, Zhan X, Guo W, Song Z, Liu Y, Hiess F, Boyce AKJ, Ni M, Wang R, Ter Keurs H, Back TG, Fill M, Thompson RJ, Turner RW, Gordon GR, Chen SRW (2020) Limiting RyR2 open time prevents Alzheimer's disease-related neuronal hyperactivity and memory loss but not β-amyloid accumulation. Cell Rep 32:108169.
Ye X, Sun X, Starovoytov V, Cai Q (2015) Parkin-mediated mitophagy in mutant hAPP neurons and Alzheimer's disease patient brains. Hum Mol Genet 24:2938–2951.
Yu WH, Cuervo AM, Kumar A, Peterhoff CM, Schmidt SD, Lee JH, Mohan PS, Mercken M, Farmery MR, Tjernberg LO, Jiang Y, Duff K, Uchiyama Y, Näslund J, Mathews PM, Cataldo AM, Nixon RA (2005) Macroautophagy—a novel β-amyloid peptide-generating pathway activated in Alzheimer's disease. J Cell Biol 171:87–98.
Zhang H, Sun S, Herreman A, De Strooper B, Bezprozvanny I (2010) Role of presenilins in neuronal calcium homeostasis. J Neurosci 30:8566–8580.
Zhang H, Sun S, Wu L, Pchitskaya E, Zakharova O, Fon Tacer K, Bezprozvanny I (2016) Store-operated calcium channel complex in postsynaptic spines: a new therapeutic target for Alzheimer's disease treatment. J Neurosci 36:11837–11850.
Zhang ZG, Yang XF, Song YQ, Tu J (2021) Autophagy in Alzheimer's disease pathogenesis: therapeutic potential and future perspectives. Ageing Res Rev 72:101464.